

Kinematical relativistic effects in $(\vec{e}, e'\vec{N})$ reactions

M.C. Martínez¹, J.A. Caballero¹, T.W. Donnelly²

¹*Departamento de Física Atómica, Molecular y Nuclear
Universidad de Sevilla, Apdo. 1065, E-41080 Sevilla, SPAIN*

²*Center for Theoretical Physics, Laboratory for Nuclear Science and Department of Physics
Massachusetts Institute of Technology, Cambridge, MA 02139, USA*

Abstract

Kinematical relativistic effects are analyzed within the plane-wave impulse approximation for outgoing nucleon polarized responses in coincidence electron scattering. Following recent approaches for semi-relativistic reductions of the electromagnetic current operator, here an exact treatment of the problem for the transferred energy and momentum is presented. Rather than employing existing semi-relativistic expressions for the single-nucleon matrix elements, in this work the response functions are expanded directly. Results are compared for different kinematical situations with the fully-relativistic PWIA calculation as well as with previous expansions. Off- and 'on-shell' prescriptions are also studied in detail, and a systematic analysis of the various kinematical variables involved in the process is presented.

PACS: 25.30.Rw, 14.20.Gk, 24.10.Jv, 24.30.Gd, 13.40.Gp *Keywords:* Nuclear reactions; Coincidence electron scattering; Polarized responses; Transferred polarization asymmetries; Semi-relativistic expansions; On- and off-shell prescriptions.

MIT/CTP#3214

1 Introduction

The starting point for many analyses of coincidence electron scattering reactions invokes the plane-wave impulse approximation (PWIA). Here a single nucleon in the nucleus absorbs the total energy and momentum transferred by the virtual photon (Born approximation), and is subsequently ejected without interacting with the residual nucleus. Obviously, PWIA is an oversimplified description of the reaction mechanism. Other ingredients such as final-state interactions (FSI), Coulomb distortion of the electrons, two-body correlations, ... can be important when making detailed comparisons with experimental data. However, the great advantage of PWIA is that it allows one to simplify and clarify the essential physics issues underlying the problem. Indeed, some observables can be shown to be rather insensitive to FSI and other distortion effects and effects beyond the impulse approximation are minimal for well-chosen kinematical conditions, and thus PWIA calculations may sometimes be adequate.

A large fraction of past theoretical work on $(e, e'N)$ reactions was carried out on the basis of non-relativistic calculations. Within this scheme, the bound and ejected nucleons are described by non-relativistic wave functions which are solutions of the Schrödinger equation with phenomenological potentials. The current operator is also described by a non-relativistic expression derived directly from a Pauli reduction that begins with the relativistic current operator and free Dirac spinors. Such standard non-relativistic reductions have usually been based on expansions in powers of p/M_N , q/M_N and ω/M_N , where p is the missing momentum, q and ω are the momentum transfer and energy transfer, respectively, and M_N is the nucleon mass. This approach constitutes the basis for the standard distorted-wave impulse approximation (DWIA) that has been widely used to describe $(e, e'N)$ experiments performed at intermediate energies [1, 2, 3].

In the last decade, given new higher-energy facilities, some experiments performed have involved momenta and energies that are high enough to invalidate the non-relativistic expansions assumed in DWIA. Thus, a consistent description of these processes requires one to incorporate relativistic degrees of freedom wherever possible [4, 5]. For example, nuclear responses and cross sections have been investigated recently using the relativistic mean field approach [6, 7, 8, 9, 10]. This constitutes the basis of the relativistic distorted-wave impulse approximation (RDWIA), where bound and scattered wave functions are described as Dirac solutions with scalar and vector potentials, and the relativistic free nucleon current operator is assumed. So far, RDWIA calculations have clearly improved the comparison with experimental data over the previous non-relativistic approaches [6, 7, 8, 9, 10, 11].

Following the discussion presented in previous work [9, 10, 12], relativistic effects can be cast into two general categories: kinematical and dynamical effects. Dynamical relativistic effects come from the difference between the relativistic and non-relativistic nucleon wave functions. For instance, one may distinguish effects associated with the Darwin term, that mainly affects the determination of spectroscopic factors at low missing momenta [6, 7], and effects due to the dynamical enhancement of the lower components in the relativistic wave functions. These latter effects have been studied in detail in recent work within the plane-wave limit [12, 13, 14] and including also FSI between the ejected nucleon and the residual nucleus [9, 10]. In both cases the effects introduced by the presence of negative-energy components in the nucleon wave functions (which are generally significant mainly at

high missing momentum) have been also proven to be very important for specific observables even at low/moderate values of the missing momentum p . In particular, within the relativistic plane-wave impulse approximation (RPWIA), the analysis of dynamical relativistic effects is considerably simplified and analytic expressions that explicitly incorporate the contributions arising from the negative-energy components in the bound nucleon wave function can be obtained. This subject was thoroughly developed in [13] (see also [15]) for the case of unpolarized $A(e, e'N)B$ reactions, and has recently been extended to the case of recoil nucleon polarized processes [12]. The analysis of the unpolarized $(e, e'p)$ reaction including FSI was discussed in [9, 10] and its extension to $A(\vec{e}, e'\vec{N})$ will be presented in a forthcoming publication [16].

Our main interest in this paper is focused on the analysis of the kinematical relativistic effects. These are directly connected to the structure of the four-component current operator compared with the non-relativistic (two-component) expressions. The usual procedure to build the electromagnetic nuclear current operators starts by employing the on-shell single-nucleon currents. In [17] the exact on-shell operators for use between two-component spin spinors were developed. For applications to nuclear physics where nucleons are off-shell, it is necessary to make further approximations. First, the on-shell expressions for the operators can be inserted between nuclear wave functions, which are not on-shell plane waves but are the off-shell single-particle wave functions describing the nucleons interacting in nuclei. Second, the standard procedure has been to expand the expressions for the electromagnetic current in dimensionless momenta, retaining only the leading-order terms in all energies or momenta over nucleon mass. This gives rise to the standard non-relativistic limit, yielding the simple expressions obtained for the electromagnetic currents that have been commonly used for many years in DWIA analyses. Unfortunately, these approximations are not adequate in present high-energy experiments, as q and ω can be comparable to M_N .

In recent work [17, 18] new expressions for the current operators were deduced treating the transferred energy and momentum exactly while expanding only in missing momentum over nucleon mass. The results to date show that these ‘relativized’ current operators retain important relativistic aspects not taken into account in the traditional non-relativistic reductions. While we frequently continue to call this approach a non-relativistic expansion, it might be more appropriate to call it “semi-relativistic” in that part of the (kinematical) relativistic behaviour is being taken into account, leaving only a variable such as $\chi \equiv \frac{p}{M_N} \sin \theta$, where θ is the angle formed by the missing momentum \mathbf{p} and the momentum transfer \mathbf{q} in which to expand. Clearly for some circumstances χ is indeed small, whereas both q/M_N and ω/M_N are not, and it might be expected that this approach will go a long way towards incorporating at least some aspects of relativity in the analysis.

In this work we build on these ideas and deduce new relativized expressions for the polarized (and unpolarized) responses that enter in the analysis of $A(\vec{e}, e'\vec{N})B$ reactions within PWIA. In contrast to the previous analyses [17, 18] where the semi-relativistic expansion was performed at the level of the single-particle current matrix elements, here we directly expand the single-nucleon responses.

It is important to point out that, even treating the problem of the transferred energy and momentum exactly, there are ambiguities in doing the semi-relativistic expansions. Different choices of the variables in which to expand can be made, and moreover, momentum-energy

conservation relations imposed on the different kinematical variables should be treated with caution as soon as a semi-relativistic expansion is considered in one of the variables. Several options have been explored in this work and the results obtained are compared with the fully-relativistic PWIA calculation as well as with previous expansions. Our main aim is to establish how precise the semi-relativistic reduction is, and under which conditions and/or for which observables it does or does not work.

Despite such ambiguities, in this paper most of the analysis is based on the choice of the expansion variable χ as in fact there exist reasons to choose it over some of the alternatives. First, this is the variable that enters in a natural way in the fully-relativistic PWIA expressions for the unpolarized and polarized single-nucleon responses. Second, its behaviour for small values of the missing momentum, independent of the kinematics selected, allows one to be confident about the accuracy of the semi-relativistic expansion. Indeed, using χ we shall see that the various responses can be grouped in a natural way in different classes according to their leading order term χ^n . Class “0” responses correspond to those whose leading order is given by χ^0 , class “1” to leading order χ , class “2” to χ^2 , and so on. We study how “safe” we expect the semi-relativistic reductions in χ to be for the three classes of response. Third, the kinematical effects of relativity that form the basis of the present work are not the end of the story: in work being done in parallel [12] explorations are being made of dynamical relativistic effects and the same organization into classes of response appears in a natural way when χ forms the basis for the expansion strategy.

Another issue directly connected with the uncertainty introduced in the analysis of the response functions is the off-shell character of the nucleons involved in $(e, e'N)$ processes, particularly for the initial-state bound nucleon. At present, the usual way to deal with this problem is to use different *ad hoc* recipes (prescriptions) for the current operator that may include some aspects of current conservation and Lorentz covariance. In this way we may obtain some insight into the importance of the off-shell effects, although it should always be kept in mind that the off-shell problem is not really fully under control. Here we proceed in the commonly accepted way and, lacking a fundamental approach to follow, continue to invoke the familiar off-shell prescriptions.

Finally, we also explore the so-called ‘on-shell’ prescription where the bound nucleon is forced to be on-shell. This leads, from energy-momentum conservation, to an unphysical negative excitation energy. However, the important advantage of the ‘on-shell’ prescription is that it does not present either Gordon or gauge ambiguities — the current is naturally conserved. An estimate of the uncertainty introduced by the semi-relativistic reductions is provided by comparing the results obtained using the new ‘relativized’ single-nucleon responses with the ‘on-shell’ and various off-shell fully-relativistic PWIA calculations.

The present study has been undertaken in a wider context where various other aspects of the problem of treating relativistic effects in $(e, e'N)$ reactions provide the focus. Any attempt to put all of the facets of the overall study together would be far too unwieldy and accordingly the various components of our work are being presented separately. It is, however, important to understand how they interact with one another:

- The present work addresses only the issue of **kinematical** relativistic effects for responses and polarization asymmetries strictly within the context of PWIA. Both off-shell and ‘on-shell’ approaches are examined.

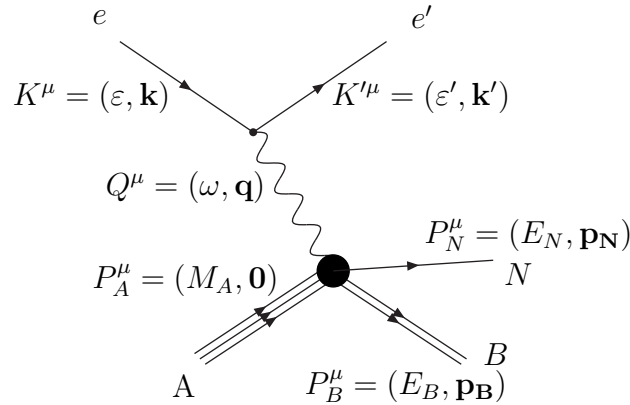


Figure 1: Feynman diagram for the $A(e, e'N)B$ process within the Born approximation.

- In an accompanying paper [12] **dynamical** relativistic effects — those stemming from having non-trivial relativistic content in the nuclear wave functions — are also studied, specifically for relativistic mean field bound-state wave functions, but with plane-wave final ejected nucleon wave functions (RPWIA).
- In work in progress [16] relativistic kinematical and dynamical effects are being addressed with all of the above ingredients plus **relativistic FSI** effects, i.e., the RDWIA.

The paper is organized as follows: in Section 2 we present the basic formalism needed to describe $A(\vec{e}, e'\vec{N})B$ reactions, paying special attention to the analysis of the kinematics involved in coincidence electron scattering reactions. We discuss various options for selecting the independent kinematical variables that completely define the $(e, e'N)$ process. The relations held by these variables coming from energy-momentum conservation are also discussed. In Section 3 we focus on the PWIA. The fully-relativistic polarized single-nucleon responses corresponding to the different off-shell prescriptions are derived, and we also introduce the ‘on-shell’ approach. In this section we also derive and discuss the semi-relativistic reductions of the responses. The various off-shell PWIA responses compared with the semi-relativistic and ‘on-shell’ results evaluated for different kinematics are presented in Section 4. Finally in Section 5 we present a summary and our conclusions.

2 Formalism for $A(\vec{e}, e'\vec{N})B$ reactions

In this section we briefly summarize the basic formalism involved in the description of $(e, e'N)$ reactions (see also [19, 20, 21]). The Feynman diagram within the Born approximation (one virtual photon exchange) is depicted in Fig. 1 and defines our conventions on energies and

momenta. Apart from assuming the Born approximation, in what follows no assumption is made about the reaction mechanism; we simply introduce the kinematical variables that completely specify the process and use energy-momentum conservation to inter-relate the various energies and momenta:

$$\mathbf{q} = \mathbf{k} - \mathbf{k}' = \mathbf{p}_N + \mathbf{p}_B \quad (1)$$

$$\omega = \varepsilon - \varepsilon' = E_B + E_N - M_A, \quad (2)$$

where the target is assumed to be at rest in the laboratory frame. The missing momentum \mathbf{p} is defined as

$$\mathbf{p} \equiv -\mathbf{p}_B = \mathbf{p}_N - \mathbf{q}, \quad (3)$$

where $p = |\mathbf{p}|$ characterizes the split in momentum flow between the detected nucleon and the unobserved daughter nucleus. The corresponding split in energy can be characterized by the excitation energy of the residual nucleus

$$\mathcal{E} \equiv E_B - E_B^0 \geq 0, \quad (4)$$

where $E_B = \sqrt{p_B^2 + M_B^2}$ and $E_B^0 = \sqrt{p_B^2 + M_B^{02}}$. Here M_B includes the internal excitation energy of the residual system, while M_B^0 is its rest mass in its ground state.

Now let us briefly discuss the set of six independent kinematical variables that completely describe the cross section for the $(e, e'N)$ process. First, explicit dependences on the electron scattering angle θ_e (through the general Rosenbluth factors) and the azimuthal angle ϕ can be isolated (see [19] for details). Once the azimuthal angle ϕ and the electron scattering angle θ_e are fixed, the $(e, e'N)$ cross section is totally specified by four kinematical variables, for instance $\{q, \omega, \mathcal{E}, p\}$. The dependences of the responses on these so-called ‘dynamical’ variables involve detailed aspects of the nuclear current matrix elements, in contrast to the dependences on θ_e and ϕ which are effectively geometric. Obviously, various alternative sets of four ‘dynamical’ variables are possible when studying specific $(e, e'N)$ reactions. In what follows we present a brief discussion of some alternatives that have advantages for specific choices of kinematics.

Let us begin assuming that the momentum and energy transferred in the process are fixed. Then, the excitation energy \mathcal{E} in terms of q , ω , p (missing momentum) and the angle θ (between \mathbf{p} and \mathbf{q}) is given by

$$\mathcal{E} = M_A + \omega - \sqrt{M_N^2 + p^2 + q^2 + 2pq \cos \theta} - \sqrt{p^2 + M_B^{02}}. \quad (5)$$

Thus there are clear relationships between the sets $\{E_N, \theta_N\}$ (θ_N being the angle between \mathbf{p}_N and \mathbf{q}) and $\{p, \theta\}$ and hence $\{\mathcal{E}, p\}$. Note that Eq. (5) yields a curve of \mathcal{E} versus p for each choice of θ , where the requirement $|\cos \theta| \leq 1$ imposes constraints on the kinematics. Let us recall what domain in the (\mathcal{E}, p) plane is compatible with the conservation of energy and momentum. First, we introduce the quasielastic peak value for the energy transfer ω_{QEP} which is given by

$$\omega_{QEP} = \sqrt{q^2 + M_N^2} + M_B - M_A. \quad (6)$$

For ω -values such that $\omega < \omega_{QEP}$ the trajectories $\cos \theta = \pm 1$ for a selected value of the momentum transfer q are plotted in the top panel in Fig. 2. Here we only show the physical

region $\mathcal{E} \geq 0$. All physically allowable values of \mathcal{E} and p must lie below the curve $\cos \theta = -1$ and, of course, above $\mathcal{E} = 0$. In contrast, in the case of the curve corresponding to $\cos \theta = +1$, the allowable values of \mathcal{E} and p must lie above this curve, and thus no physically values occur for this condition. Therefore, for $\omega < \omega_{QEP}$ the physical region is completely defined by the $\cos \theta = -1$ curve and $\mathcal{E} = 0$ (shadowed region in top panel in Fig. 2). The limit values of the missing momentum p are denoted by $p_{min} \equiv -y \geq 0$ and $p_{max} \equiv +Y$ (see [20] for the explicit expressions). Note that $\omega < \omega_{QEP}$ then implies that $y < 0$.

The case $\omega > \omega_{QEP}$ is shown in the bottom panel in Fig. 2. Here the $\cos \theta = -1$ curve is similar, except that now p_{min} is negative and so y is positive. As in the previous case the physically allowable region must lie below the $\cos \theta = -1$ curve and above the $\cos \theta = +1$ curve. Note however that the latter condition does enter in the quadrant where $\mathcal{E} \geq 0$ and $p \geq 0$, providing a new boundary condition (see shadowed region).

In both cases (positive and negative y -regions) the value of the energy transfer ω is completely specified in terms of q and y

$$\omega(q, y) = \sqrt{M_N^2 + (q + y)^2} + \sqrt{y^2 + M_B^2} - M_A, \quad (7)$$

where $\omega = \omega_{QEP}$ occurs for $y = 0$. Thus, the set of four ‘dynamical’ variables might be chosen as $\{q, \omega, E_N, \theta_N\}$, $\{q, \omega, \mathcal{E}, p\}$ or equivalently (sometimes more conveniently) $\{q, y, \mathcal{E}, p\}$.

Having set up the general kinematics involved in coincidence electron scattering reactions, next we consider briefly the general form for the coincidence cross section with the incident electron beam and outgoing nucleon both polarized. Within the Born approximation, the general cross section in the laboratory system can be written as

$$\frac{d\sigma}{d\varepsilon' d\Omega_e d\Omega_N} = \frac{2\alpha^2}{Q^4} \left(\frac{\varepsilon'}{\varepsilon} \right) K f_{rec}^{-1} \eta_{\mu\nu} W^{\mu\nu}, \quad (8)$$

with K a kinematical constant given by $K = p_N M_N M_B / M_A$, α is the fine structure constant, $\eta_{\mu\nu}$ is the familiar leptonic tensor that can be evaluated directly using trace techniques [19], and $W^{\mu\nu}$ is the hadronic tensor containing all of the nuclear structure and dynamics information. The latter is given directly in terms of the nuclear electromagnetic transition currents in momentum space.

Using the general properties of the leptonic tensor, it may be shown that the contraction of the leptonic and hadronic tensors can be decomposed in terms of leptonic kinematical ‘super-Rosenbluth’ factors and response functions. The differential cross section may then be written

$$\frac{d\sigma}{d\Omega_e d\varepsilon' d\Omega_N} = K \sigma_M f_{rec}^{-1} \left[v_L R^L + v_T R^T + v_{TL} R^{TL} + v_{TT} R^{TT} + h \left(v_{T'} R^{T'} + v_{TL'} R^{TL'} \right) \right], \quad (9)$$

where f_{rec} is the usual recoil factor [19] and σ_M is the Mott cross section. The kinematic factors v_α contain all of the dependence on the leptonic vertex aside from overall multiplicative factors (see [19] for their explicit expressions in the extreme relativistic limit (ERL)). The factor $h = \pm 1$ is the incident electron’s helicity. The hadronic current enters via the response functions R^α . The labels L and T refer to projections of the current matrix elements longitudinal and transverse to the virtual photon direction, respectively.

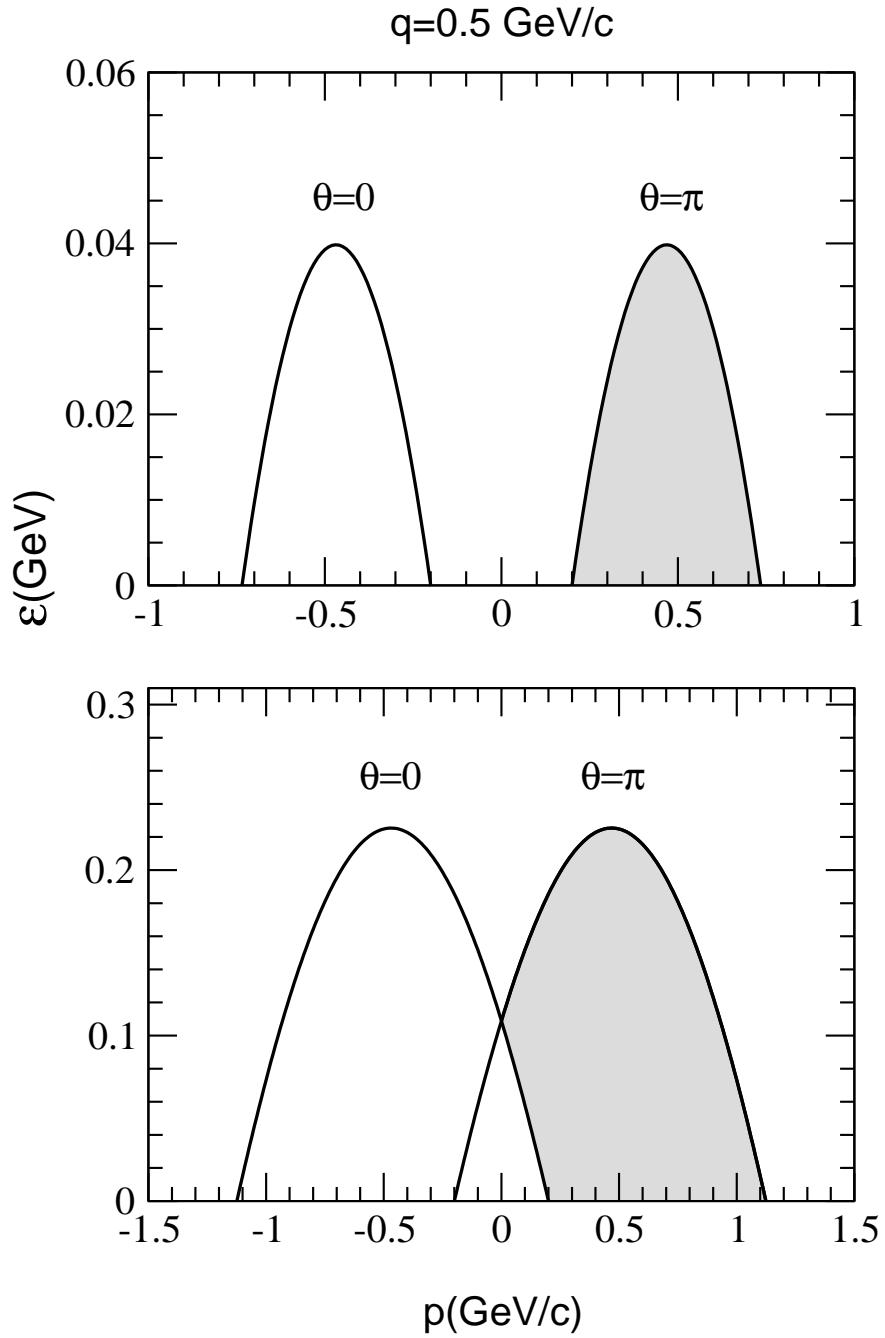


Figure 2: Excitation energy as a function of the missing momentum p for the process $^{16}\text{O}(e, e'p)^{15}\text{N}$. In the top panel the momentum transfer q is fixed to $q = 0.5 \text{ GeV/c}$ and $\omega = 55.0 \text{ MeV} < \omega_{QEP}$, while in the bottom panel it is taken to be $\omega = 240.6 \text{ MeV} > \omega_{QEP}$.

In the case of $A(\vec{e}, e'\vec{N})B$ reactions, the hadronic response functions are usually given by referring the recoil nucleon polarization to the coordinate system defined by the axes¹: \mathbf{l} (parallel to the momentum \mathbf{p}_N of the outgoing nucleon), \mathbf{n} (perpendicular to the plane containing \mathbf{p}_N and the momentum transfer \mathbf{q}), and \mathbf{s} (determined by $\mathbf{n} \times \mathbf{l}$). A total of eighteen response functions enter in the general analysis of $A(\vec{e}, e'\vec{N})B$ reactions (see [4, 5, 22] for their explicit expressions). In terms of the polarization asymmetries, the differential cross section can be expressed in the form

$$\frac{d\sigma}{d\varepsilon' d\Omega_e d\Omega_N} = \frac{\sigma_0}{2} [1 + \mathbf{P} \cdot \boldsymbol{\sigma} + h(A + \mathbf{P}' \cdot \boldsymbol{\sigma})] , \quad (10)$$

where σ_0 is the unpolarized cross section, A denotes the electron analyzing power, and \mathbf{P} (\mathbf{P}') represents the induced (transferred) polarization. A general study of the properties and symmetries of all of these responses and polarizations can be found in [4, 5]. Here, we simply note that in coplanar kinematics, $\phi = 0$, the only surviving polarization components are P_n , P'_l and P'_s .

3 Plane-Wave Impulse Approximation

The PWIA constitutes the simplest approach to describing the reaction mechanism for coincidence electron scattering reactions. It has been discussed in detail in previous work [1, 2, 3, 23], and thus here we simply summarize the basic expressions needed for the discussions to follow. The basic assumptions in PWIA are the following: i) the electromagnetic current is taken to be a one-body operator (impulse approximation), ii) the ejected nucleon is a plane wave, i.e., the nucleon emerges from the nucleus without interaction with the residual nuclear system, and iii) the nucleon detected in the coincidence reaction is the one to which the virtual photon is attached.

The analysis of $(\vec{e}, e'\vec{N})$ reactions is further simplified when FSI are neglected. The induced polarization \mathbf{P} and the analyzing power A are zero in this case [4, 5]. Thus, only the transferred asymmetry \mathbf{P}' survives in the plane-wave limit. Moreover, the normal component P'_n enters only for out-of-plane kinematics. In terms of nuclear responses, from the total of eighteen response functions, only nine survive within PWIA. Four, R_0^L , R_0^T , R_0^{TL} and R_0^{TT} , represent the unpolarized responses and the five remaining, $R_l^{T'}$, $R_s^{T'}$, $R_l^{TL'}$, $R_s^{TL'}$ and $R_n^{TL'}$, depend explicitly on the recoil nucleon polarization and only enter when the electron beam is also polarized.

An important simplification of PWIA is that the cross section factorizes into two basic terms, the electron-nucleon cross section (affected by off-shell uncertainties) and the spectral function or, in the case where the daughter state is a discrete one (as in this work), the momentum distribution that provides the probability of finding a nucleon in the nucleus with given energy and momentum. Within PWIA the hadronic tensor is then given in the form

$$W^{\mu\nu} = \mathcal{W}^{\mu\nu}(\mathbf{p}, \mathbf{q})N(p) , \quad (11)$$

¹Note that for simplicity in this work we use the notation l , n , s , whereas in [19] final-state polarizations were labelled with primes, l' , n' , s' , to distinguish them from initial-state target polarizations for which the primes were absent.

where $N(p)$ represents the momentum distribution of a (non-relativistic) bound orbital, and $\mathcal{W}^{\mu\nu}$ is the tensor for elastic scattering on a free nucleon whose explicit expression can be evaluated directly using trace techniques [13, 23]. It is crucial to point out that the factorization result in Eq. (11) is only strictly valid if the dynamical enhancement of the negative-energy components in the bound wave function is neglected, i.e., if the bound wave function is expanded in terms of free positive-energy Dirac spinors u alone. The contribution of the negative-energy components gives rise to the relativistic plane-wave impulse approximation (RPWIA) and destroys the factorization property (see [12, 13, 14]).

The differential cross section can be written in PWIA as

$$\frac{d\sigma}{d\Omega_e d\varepsilon' d\Omega_N} = K f_{rec}^{-1} \sigma^{eN} N(p), \quad (12)$$

with σ^{eN} the electron-nucleon cross section that can be decomposed into single-nucleon response functions according to

$$\sigma^{eN} = \frac{2\alpha^2 \varepsilon'}{Q^4 \varepsilon} \eta_{\mu\nu} \mathcal{W}^{\mu\nu}(\mathbf{p}, \mathbf{q}) = \sigma_M \left[\sum_{\alpha=L,T,TL,TT} v_\alpha \mathcal{R}^\alpha + h \sum_{\alpha'=T',TL'} v_{\alpha'} \mathcal{R}^{\alpha'} \right]. \quad (13)$$

The hadronic response functions in PWIA are then given simply as the product of the single-nucleon responses introduced above, \mathcal{R}^α , and the (non-relativistic) momentum distribution $N(p)$.

Although FSI and dynamical relativity (even in the plane-wave limit) in general destroy the factorization property, Eq. (11) is still usually the basis for defining an effective spectral function (also called reduced cross section) which is employed to analyze and interpret experimental data.

3.1 Polarized off-shell single-nucleon responses

Within the plane-wave limit, the analysis of $(e, e'N)$ reactions involves the half-off-shell γNN vertex. From parity and time reversal transformation properties together with Lorentz and gauge invariance, this may be shown to involve four form factors that depend not only on Q^2 but also on the invariant mass P^2 [24]. At present, a rigorous approach to treating the off-shell dependences does not exist, and thus it is necessary to rely on simple *ad hoc* prescriptions. This is the scheme initially developed by de Forest [25] and later on generalized to more complex (polarized) situations [23].

More specifically, the de Forest procedure involves the three following basic steps: first, the spinors are treated as free (on-shell) ones; second, the current operator is chosen to be the on-shell one. Here two forms, called *CC1* and *CC2*, have commonly been assumed

$$\Gamma_{CC1}^\mu = (F_1 + F_2)\gamma^\mu - \frac{F_2}{2M_N}(\bar{P} + P_N)^\mu \quad (14)$$

$$\Gamma_{CC2}^\mu = F_1\gamma^\mu + \frac{iF_2}{2M_N}\sigma^{\mu\nu}Q_\nu, \quad (15)$$

where F_1 and F_2 are the Pauli and Dirac form factors, respectively, that depend only on Q^2 , and the on-shell variable $\bar{P}^\mu = (\bar{E}, \mathbf{p})$ with $\bar{E} = \sqrt{p^2 + M_N^2}$ has been introduced. Note

that the $CC1$ operator is obtained from the $CC2$ one by using the Gordon decomposition (only valid for free on-shell nucleons). In PWIA, however, the two current operators are in general different because of the off-shell bound nucleon involved in the process. Finally, the matrix elements of the operators $CC1$ and $CC2$ violate conservation of the one-body current (impulse approximation). Thus, six different possibilities to deal with the half-off-shell γNN vertex are commonly involved. They are connected with the form of the current operator selected, and how current conservation is imposed or not (choice of gauge). These six off-shell prescriptions are denoted by: i) $NCC1$ and $NCC2$, where no current conservation is imposed (Landau gauge), ii) $CC1^{(0)}$ and $CC2^{(0)}$, where current conservation is imposed by eliminating the longitudinal component (Coulomb gauge), and iii) $CC1^{(3)}$ and $CC2^{(3)}$, where current conservation is imposed by eliminating the time component (Weyl gauge). One hopes that the differences found between the results obtained with these prescriptions may allow one to estimate the uncertainty introduced by the off-shell effects in $(e, e'N)$ reactions, although it should always be kept in mind that these are merely prescriptions for off-shell behaviour, albeit popular ones.

Using trace techniques the polarized recoil single-nucleon tensor introduced in Eq. (11) is simply given by

$$\mathcal{W}^{\mu\nu} = \frac{1}{8M_N^2} \text{Tr} \left[\hat{\Gamma}^\mu (\bar{\mathcal{P}} + M_N) \bar{\Gamma}^\nu (1 + \gamma_5 \not{S}_N) (\mathcal{P}_N + M_N) \right], \quad (16)$$

where we have introduced the recoil nucleon spin projector $(1 + \gamma_5 \not{S}_N)/2$ and use the notation $\bar{\Gamma}^\mu = \gamma^0 \Gamma^\mu \gamma^0$. From Eq. (16) it is clear that all antisymmetric contributions come from the γ_5 term, and thus the single-nucleon tensor can be decomposed into its symmetric and antisymmetric parts

$$\mathcal{W}^{\mu\nu} = \mathcal{S}^{\mu\nu} + \mathcal{A}^{\mu\nu}(S_N), \quad (17)$$

with all of the dependence on the recoil nucleon polarization contained solely in the antisymmetric tensor. When contracted with the leptonic tensor, the symmetric term, $\mathcal{S}^{\mu\nu}$, gives rise to the electron-unpolarized single-nucleon responses, whereas the antisymmetric contribution, $\mathcal{A}^{\mu\nu}(S_N)$, is to be contracted with the antisymmetric (polarized) term in the leptonic tensor. Thus, within PWIA the recoil nucleon polarization enters only in the electron-polarized responses. Explicit expressions for the single-nucleon tensor $\mathcal{W}^{\mu\nu}$ for the two forms of the current operator in Eqs. (14,15) are presented in Appendix A.

The various single-nucleon response functions that enter in $(\vec{e}, e'\vec{N})$ reactions are constructed directly as components of the single-nucleon tensor in Eq. (17) according to

$$\mathcal{R}^L = \left(\frac{q^2}{Q^2} \right)^2 \left[\mathcal{S}^{00} - 2\frac{\omega}{q} \mathcal{S}^{03} + \frac{\omega^2}{q^2} \mathcal{S}^{33} \right] \quad (18)$$

$$\mathcal{R}^T = \mathcal{S}^{22} + \mathcal{S}^{11} \quad (19)$$

$$\mathcal{R}^{TL} = \frac{q^2}{|Q^2|} 2\sqrt{2} \left[\cos \phi \left(\mathcal{S}^{01} - \frac{\omega}{q} \mathcal{S}^{31} \right) - \sin \phi \left(\mathcal{S}^{02} - \frac{\omega}{q} \mathcal{S}^{32} \right) \right] \quad (20)$$

$$\mathcal{R}^{TT} = (\mathcal{S}^{22} - \mathcal{S}^{11}) \cos 2\phi + 2\mathcal{S}^{12} \sin 2\phi \quad (21)$$

$$\mathcal{R}^{T'} = -2\mathcal{A}^{12} \quad (22)$$

$$\mathcal{R}^{TL'} = \frac{q^2}{Q^2} 2\sqrt{2} \left[\sin \phi \left(\mathcal{A}^{01} - \frac{\omega}{q} \mathcal{A}^{31} \right) + \cos \phi \left(\mathcal{A}^{02} - \frac{\omega}{q} \mathcal{A}^{32} \right) \right], \quad (23)$$

where the labels $\{1, 2, 3\}$ refer to the three usual directions that determine the nucleonic plane (see [19, 23] for details). Note that if gauge invariance is fulfilled, implying that $\mathcal{W}^{03} = \mathcal{W}^{30} = (\omega/q)\mathcal{W}^{00}$ and $\mathcal{W}^{33} = (\omega/q)^2\mathcal{W}^{00}$, then the longitudinal and interference transverse-longitudinal responses can be written uniquely in terms of the time or longitudinal components alone. As mentioned above, in PWIA the current is not conserved and thus the results depend on how the responses are constructed from the tensor.

Analytic expressions for the polarized single-nucleon responses corresponding to the *CC1* and *CC2* current operators and the Coulomb gauge, i.e., imposing current conservation by substituting the longitudinal component in terms of the time component, are displayed in Appendix A. The explicit expressions for the unpolarized and target-polarized single-nucleon responses are given in [23].

Note that the normal contribution only enters in the interference *TL'* response for out-of-plane kinematics. In this work, all of the analysis is performed for co-planar kinematics, and thus only four responses are available within PWIA. Finally, although explicit expressions for the responses are only displayed for the two Coulomb gauge prescriptions (see Appendix A), in this work we also explore and present results corresponding to the Landau and Weyl gauges with both choices of the current operator.

3.2 The ‘on-shell’ prescription

In [17, 26] the exact on-shell operators for use between two-component spin spinors were developed. As explained in the previous section, the usual procedure to deal with off-shellness starts from current operators taken on-shell. However, when matrix elements are computed using bound initial wave functions, a basic problem occurs that persists in the analysis of the off-shell γNN vertex, namely, the breaking of gauge invariance. Current conservation of the one-body current is violated to a degree that depends on the amount of off-shellness, characterized by the energy difference $(\omega - \bar{\omega})$. In this section we consider an alternative approach, called the ‘on-shell’ prescription, which avoids this kind of ambiguity, but at the same time requires the physical missing energy to be replaced by an effective value. Hence, the ‘on-shell’ prescription should be simply considered as a different way to deal with the γNN vertex involved in $(e, e'N)$ processes.

The basic idea involved in the ‘on-shell’ approach is to force the bound nucleon to be on-shell. This means that its energy and momentum are given by the free relation, $E \equiv \bar{E} = \sqrt{p^2 + M_N^2}$. From energy conservation in $(e, e'N)$ processes (see Section 2), the excitation energy \mathcal{E} that results in this case is given by

$$\mathcal{E} = M_A - \sqrt{p^2 + M_N^2} - \sqrt{p^2 + M_B^{02}} \quad (24)$$

$$= - \left[E_S + \left(\sqrt{p^2 + M_N^2} - M_N \right) + \left(\sqrt{p^2 + M_B^{02}} - M_B^0 \right) \right] < 0, \quad (25)$$

where $E_S \equiv M_N + M_B^0 - M_A$ is the separation energy, i.e., the minimum energy needed to separate the nucleus *A* into a nucleon and the residual nucleus *B* in its ground state.

Thus, the excitation energy and the bound nucleon momentum are no longer independent, $\mathcal{E} = \mathcal{E}(p)$, and consequently one must be very careful to be consistent when calculating all of the remaining kinematical variables. Note that the excitation energy as function of p is proven to be negative for all p -values. Its absolute value gets larger as p increases, being equal to $-E_S$ for $p = 0$. Obviously, these results do not correspond to a physical situation; the physical excitation energy, $\mathcal{E} \equiv E_B - E_B^0$, is defined in a way that requires it to be positive or zero. It is important to remark that the unphysical result given by Eq. (25) is consistent with the ambiguities introduced via the different off-shell prescriptions where the excitation energy has been fixed to zero. In such a case, only for $p = 0$ and $E_S = 0$ do the ‘on-shell’ and off-shell prescriptions coincide and no ambiguities appear. As the value of p goes up, the excitation energy required to be on-shell is negative (unphysical), and consequently, off-shellness uncertainties appear, and the higher the p -value the more important they are. Below we also present observables corresponding to the ‘on-shell’ approach. How these results differ from the off-shell ones may provide us with some estimate of the uncertainties inherent in the treatment of the γNN vertex in $(e, e'N)$ reactions.

3.3 Semi-relativistic reductions

For a long time the standard procedure to treat $(e, e'N)$ reactions has been based on a non-relativistic description of the hadronic current. Bound nucleon wave functions have been described as solutions of the Schrödinger equation. Similarly, in DWIA a non-relativistic treatment of FSI has been invoked in describing the ejected nucleon wave function. Most nuclear models have been derived within such a non-relativistic framework, and hence, in order to be consistent with such descriptions of the states, one is also forced to perform some type of non-relativistic reduction of the relativistic electromagnetic current.

The standard procedure to derive non-relativistic expressions for the electromagnetic current operators has been based on expansions in all of the independent dimensionless variables, i.e., energy and momentum transfer, $\lambda = \omega/2M_N$, $\kappa = q/2M_N$, and initial-state struck nucleon momentum, p/M_N . Treating all of these as small is not justified in present studies where q and ω are comparable to the nucleon mass. Hence, here we treat the problem exactly for the transferred energy and momentum. This analysis follows closely the reductions already presented in some previous papers [17, 18, 26] — again, as noted in the introduction, these should really be called “semi-relativistic” approaches, since much of the relativistic content is not approximated. In this work, instead of making use of semi-relativistic expressions for the single-particle current matrix elements, we directly expand the various (polarized and unpolarized) single-nucleon responses starting from the fully-relativistic $CC1^{(0)}$ PWIA expressions. Moreover, various semi-relativistic expansion alternatives are explored. Our main aim is to establish how precise the semi-relativistic reductions are, and under which conditions and/or for which observables they may or may not work.

Let us start by developing in detail the semi-relativistic expansion procedures. We consider three possible choices of the variable in which to make the semi-relativistic expansion: $\chi \equiv (p/M_N) \sin \theta$, $\chi' \equiv (p/M_N) \cos \theta$ and $\eta \equiv (p/M_N)$. The transferred energy and momentum are treated exactly. In Fig. 3 we show the behaviour of χ , χ' and η as functions of the missing momentum p for different kinematical situations defined by $\{q, y, \mathcal{E} = 0\}$ (see

Section 2 for details on the kinematics). Throughout this work we present results over a wide range of values of p — the reader should, of course, be aware that contributions other than those from the impulse approximation may also be significant, especially for large p (work is in progress to provide relativistic treatments of such contributions). From the results in Fig. 3 one may conclude that the best variable in which to expand for the case $y \neq 0$ (away from the QEP) is χ . This is strictly valid up to a certain value of the missing momentum p where χ and χ' may cross each, after which χ' is the smaller, and hence more suitable as a choice of expansion variable. In the case of the quasielastic peak ($y = 0$), the semi-relativistic reduction is expected to be more precise if the expansion variable is chosen to be χ' , instead of χ or η . However, in order to estimate how valid a semi-relativistic expansion might be, it is crucial to know where the $(e, e'N)$ cross section or hadronic response functions are mainly located. This depends on the single-particle orbitals involved in the process. In particular, for an $\ell = 0$ shell the main location is centered around $p = 0$, whereas for $\ell = 1$ it is typically in the vicinity of $p \approx 100$ MeV/c. There one finds that χ , χ' and η are all reasonably small and accordingly expansions are likely to be good.

In this work the semi-relativistic reduction of the responses is made by expanding in powers of χ . There exist some general reasons to prefer χ over χ' or η . By looking at the relativistic PWIA expressions for the polarized single-nucleon responses in Eqs. (42-46), one realizes that χ enters as a natural variable in those expressions. The same holds for the unpolarized responses [23]. Thus, the various polarized and unpolarized responses might be classified into three basic categories: i) class “0” corresponding to responses which contain terms that begin with a finite leading-order contribution that does not depend on the variable χ , i.e. responses with finite terms proportional to χ^0 . This is the case for \mathcal{R}^L , \mathcal{R}^T , $\mathcal{R}_i^{T'}$, $\mathcal{R}_s^{TL'}$ and $\mathcal{R}_n^{TL'}$; ii) class “1” responses whose leading-order contributions are linear in χ , the case for \mathcal{R}^{TL} , $\mathcal{R}_s^{T'}$ and $\mathcal{R}_i^{TL'}$, and iii) class “2” responses with leading-order contributions proportional to χ^2 as for \mathcal{R}^{TT} . Below we shall examine how the effects of terms in the expansions that are of higher order than the power that characterizes the class influence the results, that is, whether or not a correlation exists between the class and the relative importance of these higher-order terms. In context it should also be mentioned that correlations with class number can also be made when examining dynamical (versus kinematical) relativistic effects [12, 13].

Now let us proceed in detail to the semi-relativistic reduction of the single-nucleon responses using χ as expansion variable. We assume co-planar kinematics, i.e., $\phi = 0$. Following the discussion in Section 2, the $(e, e'N)$ process is determined by four ‘dynamical’ variables. One is taken as the excitation energy \mathcal{E} fixed to zero, i.e., the residual nucleus is taken to be in its ground state, and another is the variable χ used to perform the semi-relativistic expansion. The two remaining ‘dynamical’ variables might be selected as $\{\kappa, \lambda\}$ or equivalently $\{\kappa, y\}$. In this work, we explore the semi-relativistic expansion for selected values of κ and y . Note that all of the remaining kinematical variables that may be introduced in the description of $(e, e'N)$ responses are given in terms of κ , y , \mathcal{E} and χ . Hence, within the semi-relativistic procedure developed in this work, they are simply evaluated as a Taylor expansion in powers of χ .

After some algebra, keeping κ , y and \mathcal{E} constant ($\mathcal{E} = 0$ here), the semi-relativistic expressions for the single-nucleon responses up to first order in powers of χ are given as

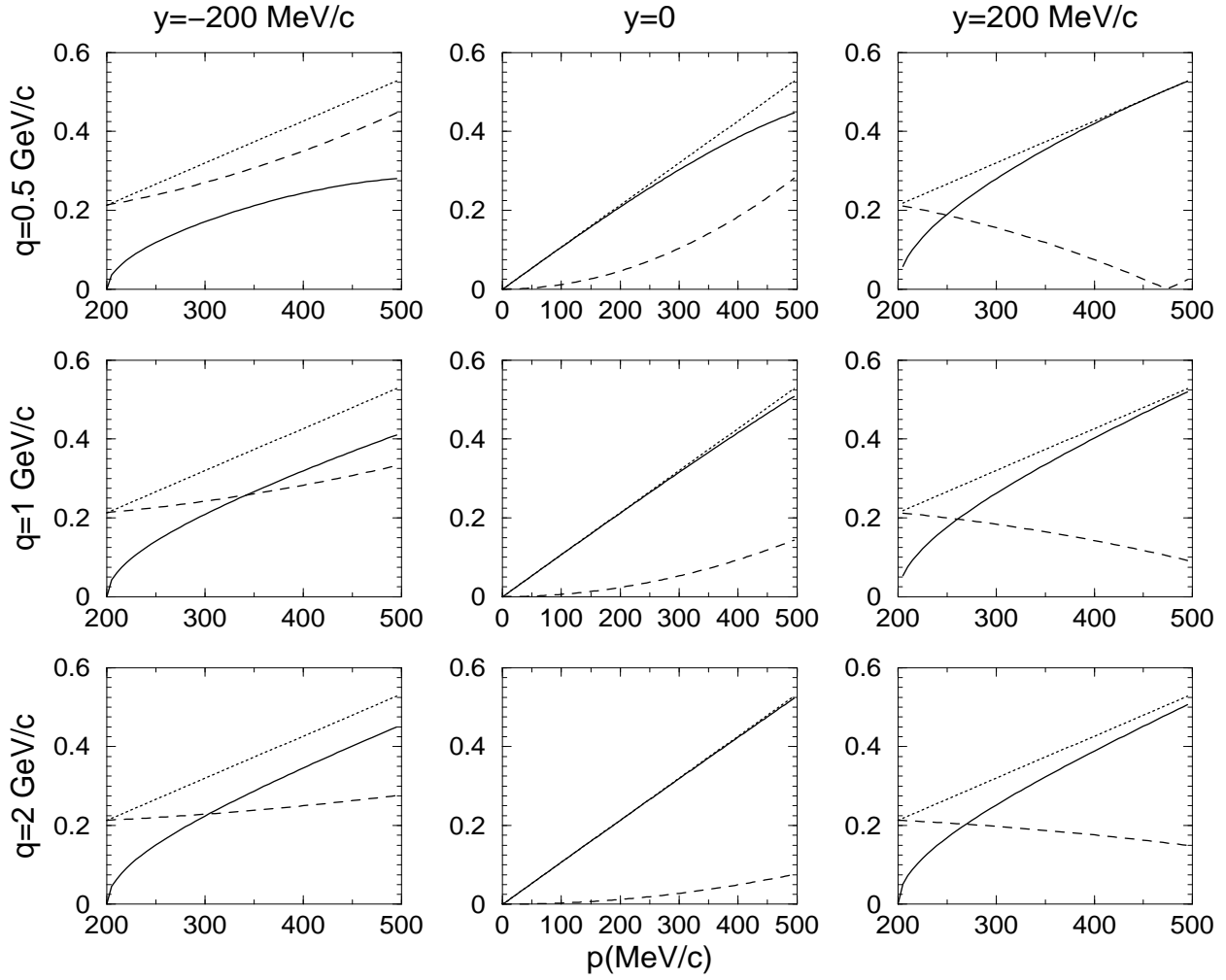


Figure 3: Behaviour of the kinematic variables χ (solid lines), $|\chi'|$ (dashed lines) and η (dotted lines) as functions of the missing momentum p for various values of q and y .

follows

$$\mathcal{R}^L = \frac{\kappa^2}{\bar{\tau}_y} (F_1 - \bar{\tau}_y F_2)^2 + \mathcal{O}(\chi^2) \quad (26)$$

$$\mathcal{R}^T = 2\bar{\tau}_y G_M^2 + \mathcal{O}(\chi^2) \quad (27)$$

$$\mathcal{R}^{TL} = 2\chi \sqrt{\frac{2\kappa^2(1 + \bar{\tau}_y)}{\bar{\tau}_y}} (F_1^2 + \bar{\tau}_y F_2^2) \cos \phi + \mathcal{O}(\chi^3) \quad (28)$$

$$\mathcal{R}^{TT} = -\chi^2 (F_1^2 + \bar{\tau}_y F_2^2) \cos 2\phi + \mathcal{O}(\chi^4) \quad (29)$$

$$\mathcal{R}_l^{T'} = 2\bar{\tau}_y G_M^2 + \mathcal{O}(\chi^2) \quad (30)$$

$$\mathcal{R}_l^{TL'} = 2\sqrt{2}\chi\kappa a G_M \left(eF_1 + \sqrt{\kappa^2 - \bar{\tau}_y} F_2 \right) \cos \phi + \mathcal{O}(\chi^3) \quad (31)$$

$$\mathcal{R}_s^{T'} = 2\chi a G_M \left(\sqrt{\kappa^2 - \bar{\tau}_y} F_1 - \bar{\tau}_y e F_2 \right) + \mathcal{O}(\chi^3) \quad (32)$$

$$\mathcal{R}_s^{TL'} = 2\sqrt{2}\kappa G_M (F_1 - \bar{\tau}_y F_2) \cos \phi + \mathcal{O}(\chi^2), \quad (33)$$

where we use the dimensionless variables defined in Appendix A and have introduced the term $\bar{\tau}_y$ that represents the value of $\bar{\tau}$ evaluated at $p = |y|$. The factors a and e are defined as

$$a \equiv \frac{1}{\kappa + \sqrt{(1 + \bar{\tau}_y) \left(\frac{\kappa^2}{\bar{\tau}_y} - 1 \right)}} \quad (34)$$

$$e \equiv \sqrt{1 + \left[\kappa + \sqrt{(1 + \bar{\tau}_y) \left(\frac{\kappa^2}{\bar{\tau}_y} - 1 \right)} \right]^2}. \quad (35)$$

We do not show the semi-relativistic expression for the $\mathcal{R}_n^{TL'}$ response because it is absent in the case of co-planar kinematics.

Note that all of the single-nucleon responses have the following generic form:

$$\mathcal{R} = \chi^n \alpha_0 [1 + \alpha_2 \chi^2 + \mathcal{O}(\chi^4)], \quad (36)$$

where $n = 0, 1, 2$ labels the class type, namely, the general expansions involve higher-order terms in χ^2 . The leading coefficient α_0 is given in Eqs. (26-33) for all responses L, T , etc., and depends on the details of the process (form factors, kinematic factors, whether the nucleon is a proton or neutron). The relative importance of the next-to-leading order contribution at small χ is characterized by the coefficient α_2 . To get some advance insight into what will be discussed at length in the following section, we provide a few typical numbers: in particular, we take $q = 1$ GeV/c, $y = 0$ and focus on the region $p \leq 100$ MeV/c (100 MeV/c is typical of valence proton knockout from ^{16}O). We truncate all expansions above at the terms involving α_2 and find the following results:

$$\begin{aligned} \alpha_2(L, n = 0) &= 1.4 \\ \alpha_2(T, n = 0) &= 1.2 \end{aligned}$$

$$\begin{aligned}
\alpha_2(TL, n = 1) &= 0.3 \\
\alpha_2(TT, n = 2) &= 0.1 \\
\alpha_2(T'_l, n = 0) &= 1.1 \\
\alpha_2(TL'_l, n = 1) &= -0.1 \\
\alpha_2(T'_s, n = 1) &= 3.3 \\
\alpha_2(TL'_s, n = 0) &= -1.4
\end{aligned} \tag{37}$$

For instance, for $p = 100$ MeV/c one has $\chi^2 = 0.011$ and the relative importance of the higher-order terms can be read off immediately. We see that the class “0” cases have α_2 ’s of order unity and accordingly the next-to-leading order corrections are typically at the 1–2% level for $p = 100$ MeV/c. The class “1” and class “2” cases are smaller by typically a factor of a few (with the exception of the anomalous T'_s case; see below). Thus typically the coefficients α_2 are “natural”, meaning they are of order unity or somewhat smaller. Clearly when χ is very small, such expansions should be quite good, whereas when it rises to larger values (as it can) they will fail. The one anomaly is also easily explained, since for it the leading-order coefficient $\alpha_0(T'_s)$ is not “natural”, but from a cancellation of the expression in parentheses in Eq. (32) is abnormally small, implying a larger than normal role for the next-to-leading order term. In [12] a similar analysis is performed for dynamical relativistic effects to ascertain the class pattern there as well.

Comparison with other reduction schemes

As we have mentioned, various alternatives can be considered in making the semi-relativistic reductions of the responses. Here we briefly review some of them and compare with the results given in Eqs. (26-33). It is important to point out that these alternative procedures are equally valid approaches, since there is really nothing that favours one of them over another, apart from the comparison with the fully-relativistic calculation.

- In [17, 18], new ‘relativized’ current matrix elements were deduced by expanding only in powers of the bound nucleon momentum $\eta \equiv p/M_N$, whereas in [26] expansions were made in χ , but for the current matrix elements and not for the single-nucleon response functions. Following the same procedure but at the level of the single-nucleon responses instead of the on-shell current matrix elements, one can obtain on-shell expressions for the single-nucleon responses. In this case all responses are given simply in terms of χ and $\bar{\tau}$ but no explicit dependence on κ enters.
- Another alternative is to make the expansion in powers of χ , as we did in the previous section, but using as independent variables κ and $\bar{\tau}$ instead of κ and y . The results obtained are formally identical to the ones given in Eqs. (26-33), except for replacing $\bar{\tau}_y$ by $\bar{\tau}$. This semi-relativistic procedure also reduces to the previous one when the value of κ is approximated by $\kappa \approx \sqrt{\bar{\tau}(1 + \bar{\tau})}$.
- Finally, in the case of the unpolarized responses we have also explored the results obtained using the ‘relativized’ current matrix elements developed in [17, 26].

Although not shown here for simplicity, we have studied the results obtained for the unpolarized and polarized single-nucleon — actually single-proton — responses for a selected choice of kinematics where $q = 500$ MeV/c, $y = 0$ and $\mathcal{E} = 0$ (for details on the kinematics, see the next section). We find that the results obtained by using the current matrix elements developed in previous studies [17, 18, 26] are very similar to our semi-relativistic reductions except for \mathcal{R}^{TT} . This last fact can be easily explained by realizing that \mathcal{R}^{TT} is a response of order χ^2 (class “2”) and the current matrix elements used in those studies were deduced by expanding only up to first order in η . Obviously, terms of order η^0 and η^2 should be considered in the matrix elements to construct the \mathcal{R}^{TT} response.

We have also checked that the relative difference between the various semi-relativistic reductions is in general smaller than the difference with respect to the relativistic PWIA calculation. In the particular case of \mathcal{R}^{TT} the various results almost coincide. This comment also applies to the responses \mathcal{R}^{TL} and $\mathcal{R}_i^{TL'}$ where the differences between the various relativistic and semi-relativistic calculations are tiny. On the contrary, the effect introduced by the choice of the semi-relativistic expansion is more important for \mathcal{R}^L , \mathcal{R}^T , $\mathcal{R}_i^{T'}$ and $\mathcal{R}_s^{TL'}$. Nevertheless, we conclude that the various alternative semi-relativistic expansions explored produce results which are rather similar, the discrepancy being at most of the order of ~ 6 – 7% even for $p = 500$ MeV/c. Hence in what follows we present a systematic analysis of the kinematical relativistic effects by comparing the semi-relativistic results obtained by making an expansion in powers of χ fixing κ , y and \mathcal{E} (see Eqs. (26-33)) with the relativistic ‘off-shell’ PWIA results, as well as with the ‘on-shell’ prescription.

4 Results

In this section we present the results obtained for the single-nucleon response functions and transferred polarization asymmetries. Our main aim is to establish the importance of the ‘off-shell’ uncertainties and kinematical relativistic effects. Accordingly we compare results corresponding to various ‘off-shell’ prescriptions with the calculations evaluated within the ‘on-shell’ approach, as well as with the semi-relativistic reduction developed in the previous section. A systematic study is presented by analyzing different kinematical situations.

Let us recall that four ‘dynamical’ variables, whose preferred choice depends on the specifics of the $(e, e'N)$ reaction, determine the response functions. In this work we assume co-planar kinematics, i.e., $\phi = 0$, and the excitation energy is taken $\mathcal{E} = 0$. Single-nucleon responses and polarization asymmetries are shown as functions of the missing momentum p . We consider only the proton case, $(e, e'p)$.

Two different choices of kinematics have been selected:

- Kinematics specified by the ‘dynamical’ variables $\{q, y, \mathcal{E}, p\}$, i.e., the observables are evaluated for selected values of q and y . In Fig. 4 we show the allowed (\mathcal{E}, p) regions for various values of q and y . Note that the allowed p -region is different for each $\{q, y\}$ choice. The figure is intended only to show the complete range of kinematics allowed and thus to make clear the entire behaviour of the variables involved. Again, as noted above, the reader is cautioned about expecting the impulse approximation to provide a complete description for the very large values of p covered in the figure. We recall

that for the off-shell prescriptions these kinematics are equivalent to the more popular $(q - \omega)$ -constant kinematics, the corresponding value of ω for each y being calculated by means of Eq. (7).

- Parallel kinematics, i.e., the polar angle θ_N is fixed to zero (see Section 2). Two alternatives have been considered. First, the kinetic energy of the outgoing nucleon is fixed; this means that the process is described by the dynamical variables $\{p_N, \theta_N, \mathcal{E}, p\}$. Here note that varying the missing momentum p means changing the momentum transfer q . Second, the momentum transfer is fixed so that $\{q, \theta_N, \mathcal{E}, p\}$ constitute the four dynamical variables. In this case, one must change the outgoing nucleon momentum p_N in order to vary the momentum p . It is important to point out that in both of these cases the value of y coincides with p , i.e., $p = |y|$ and hence increasing p means moving far away from the quasielastic peak. Within parallel kinematics, the angle θ between \mathbf{q} and \mathbf{p} might be 0 (sometimes referred as positive p -region or strictly parallel kinematics) or 180° (negative- p or antiparallel kinematics). In the first case, $\theta = 0$, one has $p_N > q$ which corresponds to $y > 0$. In this situation, note that as p increases the transfer momentum q diminishes (for p_N -fixed) or analogously, the outgoing nucleon momentum p_N goes up (for q -fixed). For \mathbf{p} antiparallel to \mathbf{q} , i.e., $\theta = 180^\circ$, one has $p_N < q$ implying y -negative. Here, increasing p means also increasing q (p_N -fixed) or diminishing p_N (q -fixed).

4.1 Analysis of single-nucleon responses for $\{q, y\}$ -fixed kinematics

We start by showing the responses corresponding to $\{q, y\}$ -fixed kinematics. In Figs. 5-8 we present the four unpolarized responses, and likewise in Figs. 9-12 the four recoil nucleon polarized responses that enter in co-planar kinematics. For each response we present the results for three values of the momentum transfer: $q = 0.5$ GeV/ c (top panels), $q = 1$ GeV/ c (middle panels) and $q = 2$ GeV/ c (bottom panels). Three different values of y have been analyzed: $y = -200$ MeV/ c ($\omega < \omega_{QEP}$) (left panels), $y = 0$ (at the quasielastic peak) (middle panels) and $y = +200$ MeV/ c ($\omega > \omega_{QEP}$) (right panels). This provides a sampling of different situations when trying to understand how the ‘off-shell’ and relativistic effects enter in the various responses and how they vary with momentum transfer and location with respect to the QEP. For the gauge-dependent (L and TL) responses we present in each individual graph five curves that correspond to the three different ‘off-shell’ prescriptions based on the use of the $CC2$ current, the ‘on-shell’ approach (dotted line) and the semi-relativistic reduction (long-dashed line) developed in the previous section. Within the off-shell curves we distinguish the three gauges: Coulomb ($CC2^{(0)}$) (solid lines), Landau ($NCC2$) (dot-dashed) and Weyl ($CC2^{(3)}$) (short-dashed). Although not shown in these graphs (for clarity), we have also studied the behaviour of the prescriptions based on the $CC1$ current, and we comment on those results in the discussion that follows. On the contrary, in the case of the purely transverse responses (no gauge ambiguities) we show the results obtained for the two current operators: $CC1$ (thin solid lines) and $CC2$ (thick solid lines).

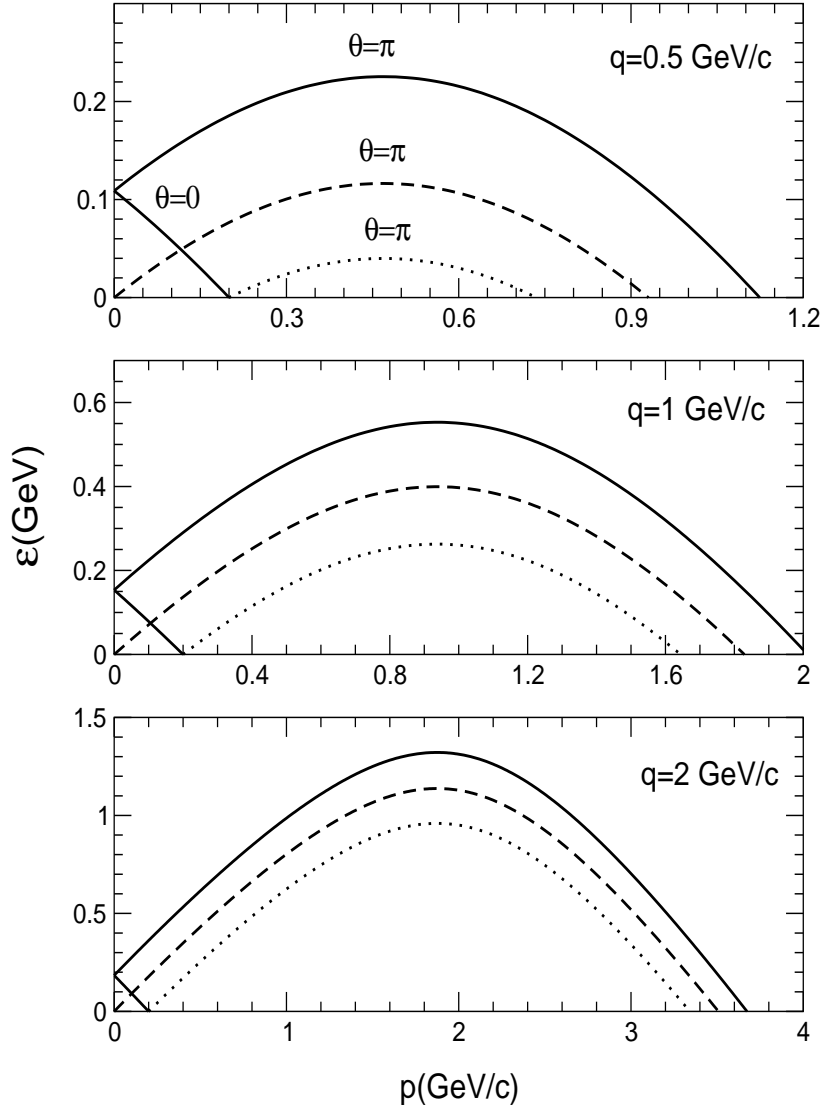


Figure 4: Excitation energy as function of p for ^{16}O . Curves are plotted for $q = 0.5, 1$ and 2 GeV/c and $y = 200$ MeV/c (solid line), $y = 0$ (dashed line) and $y = -200$ MeV/c (dotted line).

Unpolarized responses

Let us start with the analysis of the off-shell effects in the unpolarized responses (Figs. 5-8). First, we discuss the ambiguities introduced by the current operator choice. Note that although these effects are only shown in the graphs for the purely transverse responses \mathcal{R}^T and \mathcal{R}^{TT} (which only depend on the choice of the current operator), they have been also analysed for \mathcal{R}^L and \mathcal{R}^{TL} which depend additionally on the choice of gauge. Focusing on the Coulomb gauge, the effects introduced by the current operator choice are proven to be tiny for all of the responses and all of the $\{q, y\}$ -values selected, even for high missing momenta. In particular, the response \mathcal{R}^L does not depend on the current choice [23], while the Gordon uncertainties are at most of the order of $\sim 5\%$ for \mathcal{R}^{TL} and \mathcal{R}^{TT} , and less than $\sim 8-9\%$ for \mathcal{R}^T . A general dependence of the Gordon uncertainties with the energy transfer and momentum cannot clearly be extracted for the four responses. A similar discussion could be also applied to the Landau gauge. The uncertainty in this case is at most of the order of $\sim 5-6\%$, being a maximum for $y = 200$ MeV/c. In contrast, in the case of the Weyl gauge, the uncertainty associated with the current operator choice is much bigger, although it diminishes as q increases (assuming y -fixed).

In what follows we analyze the uncertainty due to the choice of gauge. As is well-known, this issue only arises for the \mathcal{R}^L and \mathcal{R}^{TL} responses. The results in Figs. 5 and 8 show that the largest differences are introduced by the Weyl gauge. This agrees with the general findings in [12, 13, 23]. On the other hand, the gauge ambiguities vary significantly with the specifics of the kinematics, i.e., the q - and y -values selected. In particular, the following general trends are observed:

- For q -fixed, the Weyl results tend to approach the results for the other two gauges as one goes from negative to positive y -values. This behaviour shows up particularly for small q . For $q = 2$ GeV/c the gauge deviations do not show any appreciable change when varying y . Moreover, the gauge uncertainties diminish significantly as q increases. Notably, this decrease is proven to be much faster for negative- y .
- The relative deviations between the Coulomb and Landau gauges increase as one moves to higher ω . The magnitude of this increase is stronger for small q -values.

To finish the discussion of the off-shell prescriptions and in order to understand the origin and significance of the relative effects discussed above, it is crucial to point out that the p -range for which the responses have been evaluated, ≤ 500 MeV/c, may represent for each $\{q, y\}$ choice a very different fraction of the total kinematically allowed p -region. In fact, as illustrated in Fig. 4, the allowed p -region is much wider as q increases. This means that $|y| \leq p \leq 500$ MeV/c may represent $\sim 55\%$ of the total p -region for $q = 500$ MeV/c (for $y = 200$ MeV/c, $\sim 30\%$), while it only represents about $\sim 9-10\%$ for $q = 2$ GeV/c. This might explain why the gauge differences discussed above are smaller for higher q .

Next we turn briefly to the ‘on-shell’ approach. We include it here for several reasons: (1) it has been used in other studies [17, 18, 26] and it is important to see how it agrees with or differs from the popular off-shell prescriptions; (2) it has the merit of providing a clear connection between current matrix elements (with corresponding current operators) and single-nucleon cross sections; and (3) it has the nice feature that current conservation

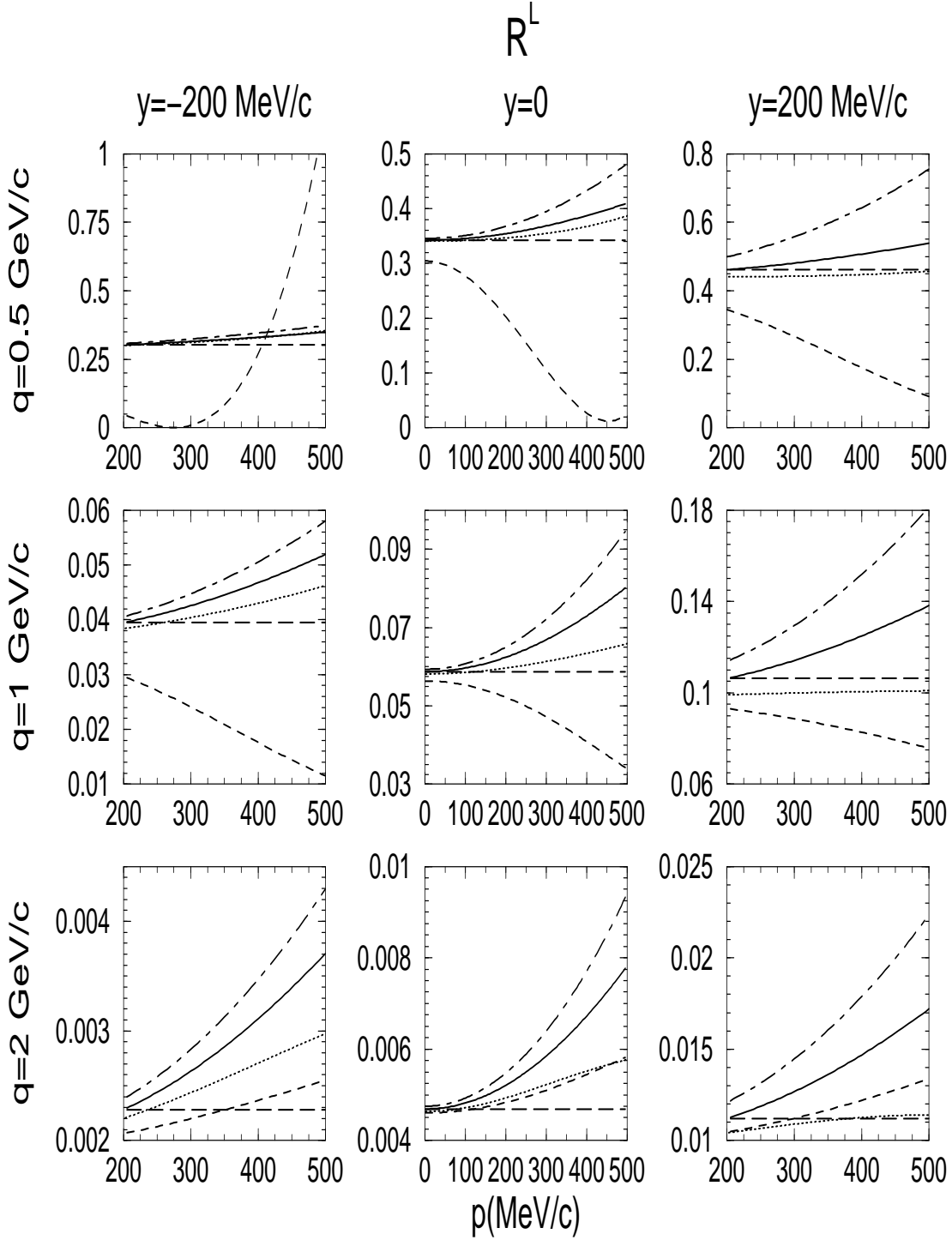


Figure 5: Unpolarized longitudinal single-nucleon response \mathcal{R}^L for $\{q, y\}$ -fixed kinematics. The excitation energy \mathcal{E} is taken to be zero. For the *CC2* off-shell prescriptions the three gauges considered are: Coulomb (solid lines), Landau (dot-dashed lines) and Weyl (short-dashed lines). The ‘on-shell’ approach is represented by dotted lines and the semi-relativistic reduction by long-dashed lines.

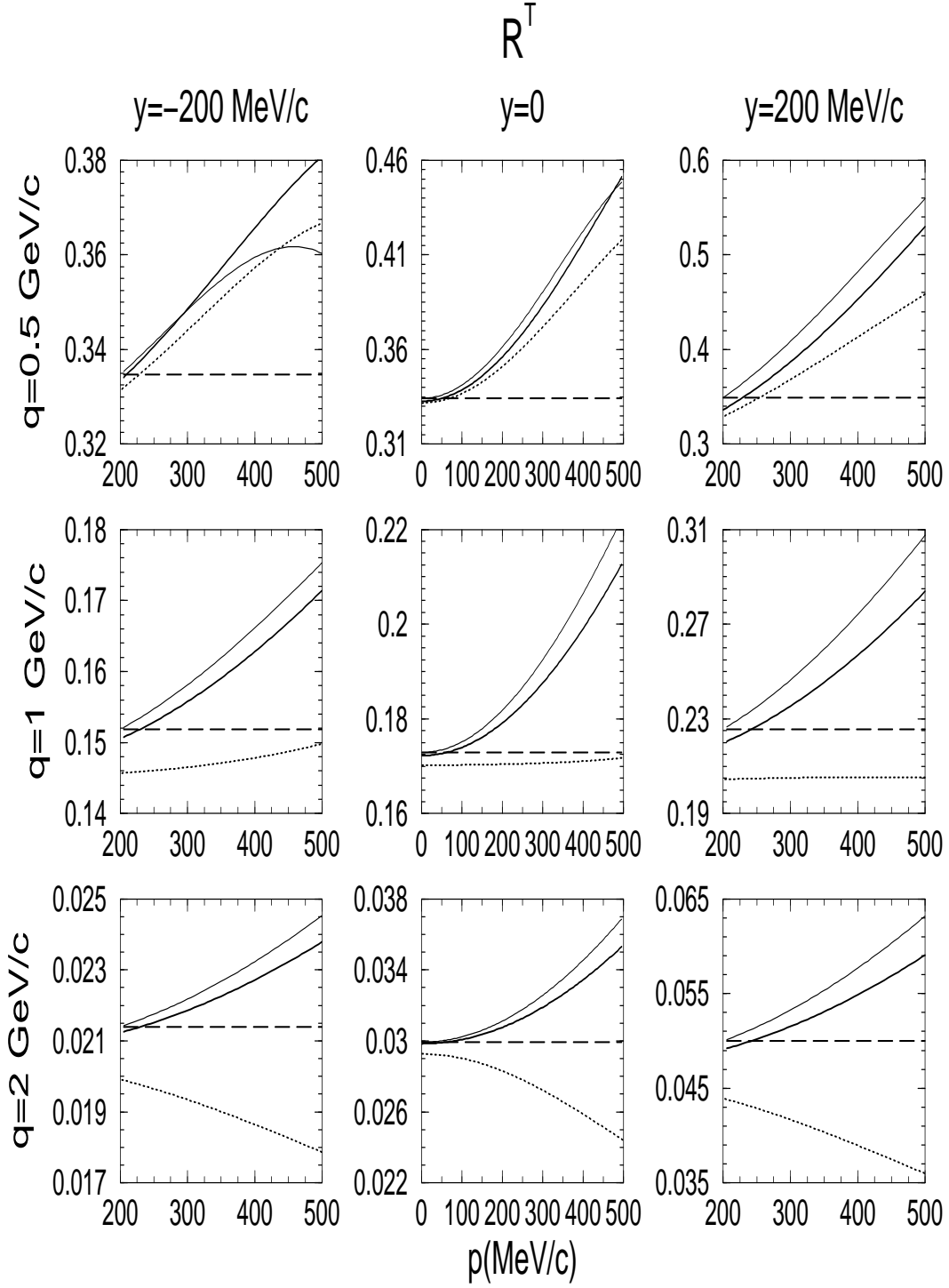


Figure 6: Same as Fig. 5, but for the \mathcal{R}^T response. We represent also the results for the $CC1$ current with thin solid lines.

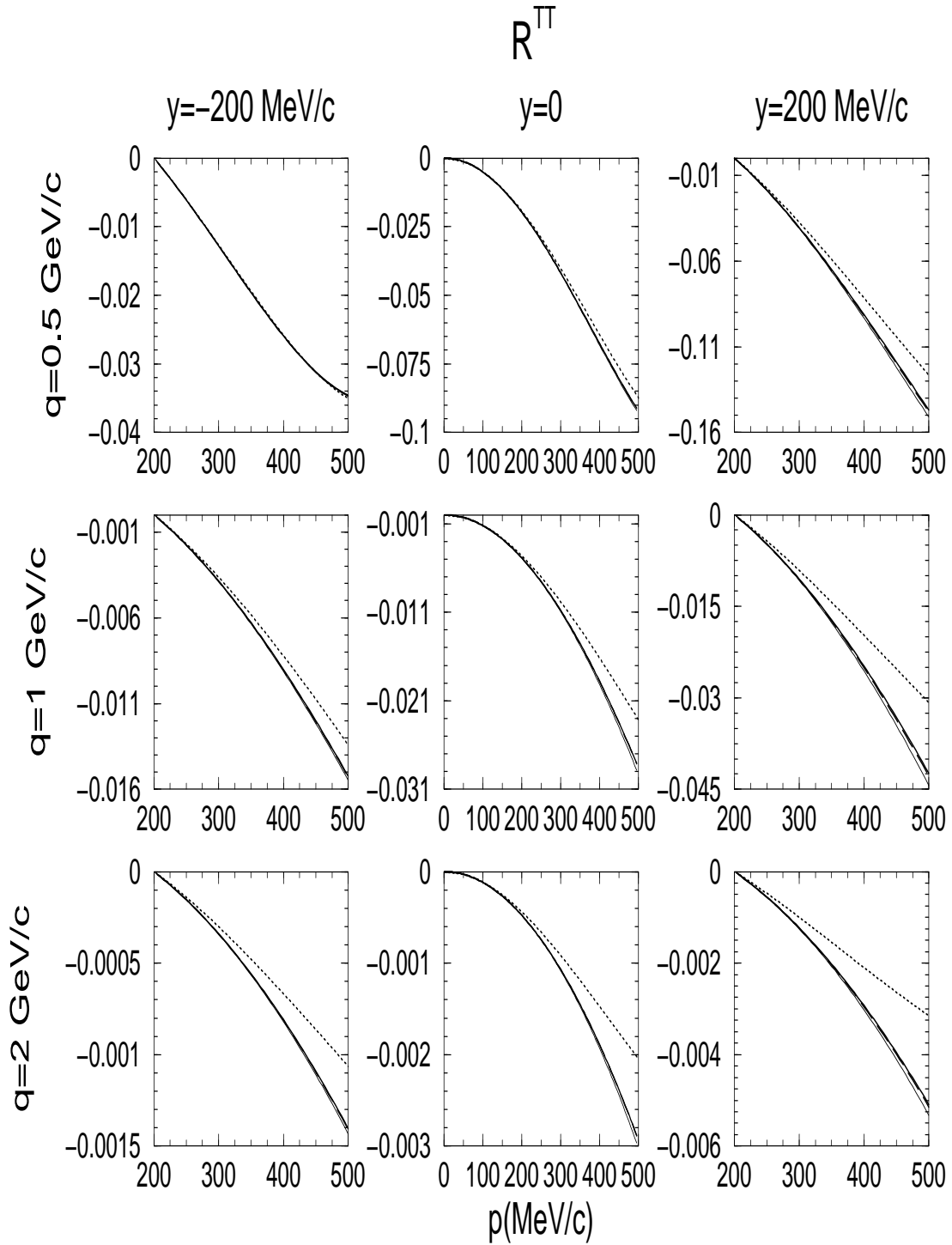


Figure 7: Same as Fig. 6, but for \mathcal{R}^{TT} .

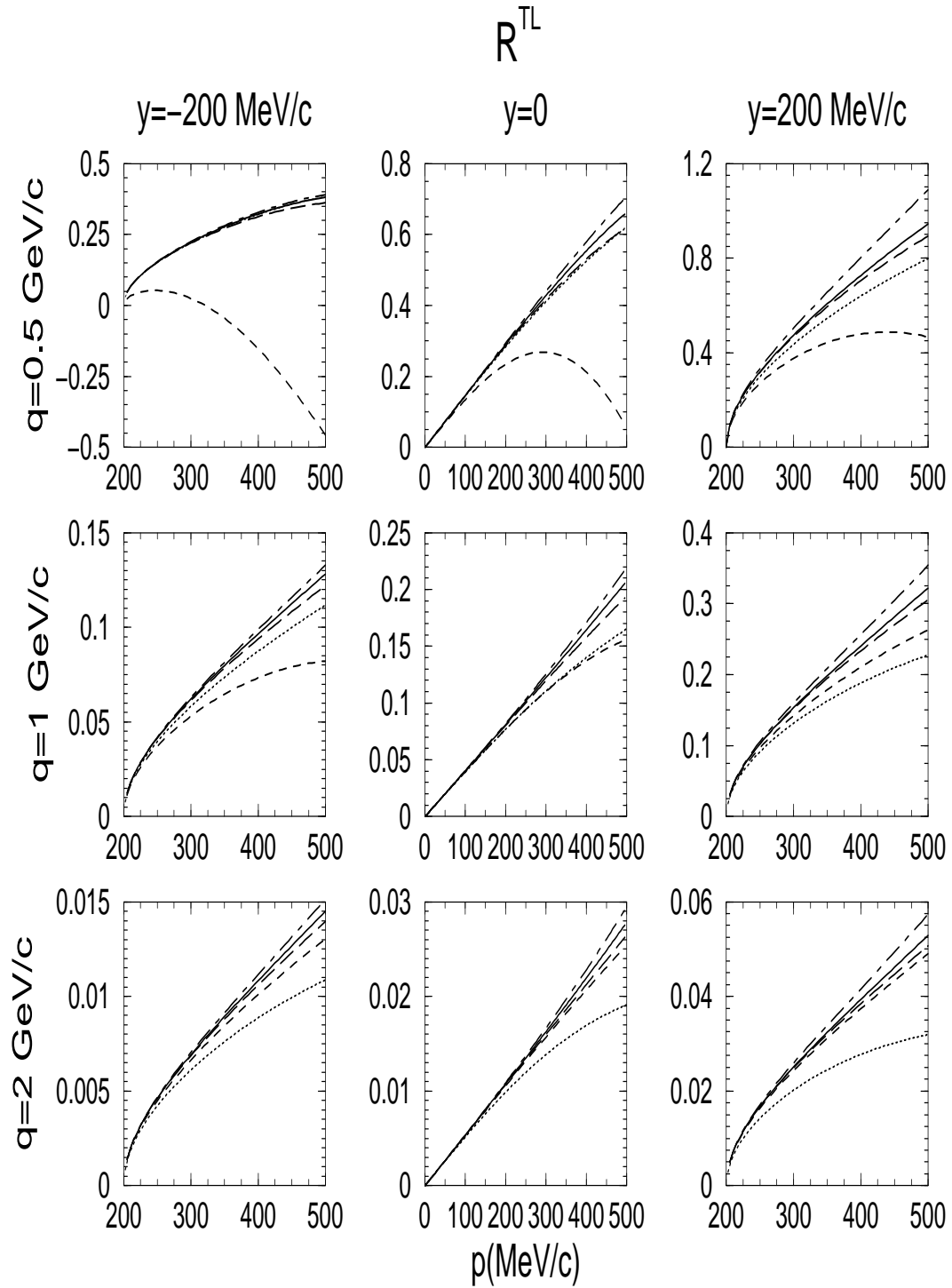


Figure 8: Same as Fig. 5, but for \mathcal{R}^{TL} .

is built in from the start and does not have to be imposed in the somewhat artificial way it does for the de Forest CC prescriptions.

The results corresponding to the ‘on-shell’ prescription are represented by dotted lines. As is seen in the figures, its deviation with respect to the off-shell prescriptions increases as the momentum and energy transfers grow (from negative to positive y -values in the latter case). This behaviour is strictly valid for the \mathcal{R}^T and \mathcal{R}^{TT} responses where gauge ambiguities do not enter, and also for the prescriptions based on the Coulomb and Landau gauges in the case of \mathcal{R}^L and \mathcal{R}^{TL} . As noted above, the Weyl results at low q differ from all other cases considered, including the ‘on-shell’ prescription.

In order to clarify the comparison between the various off-shell prescriptions and the ‘on-shell’ approach, let us state explicitly the approach taken. First, the four dynamical variables that completely determine the single-nucleon responses in general are given by $\{q, y, \mathcal{E}, p\}$. For the off-shell approaches the excitation energy is fixed ($\mathcal{E} = 0$ in this work), and once the dynamical variables $\{q, y, \mathcal{E}\}$ are given, the energy transfer ω can be evaluated. It is also usual to introduce an ‘on-shell’ transferred energy defined as $\bar{\omega} \equiv E_N - \bar{E}$, where \bar{E} is the on-shell nucleon energy, which depends only on p . For the ‘on-shell’ approach we fix $\{q, y, p\}$, determining \mathcal{E} via Eq. (25) (being forced to be an explicit function of p), then calculating the effective energy transfer $\omega_{on-shell}$ by using Eq. (7). It can be proven that the two on-shell transfer energies $\bar{\omega}$ and $\omega_{on-shell}$ do not coincide exactly; however their difference can be shown to be almost negligible for all p (at most of the order of 0.08 MeV in the case of the residual nucleus ^{15}N).

The reasons for the differences amongst the results based on the ‘on-shell’ and on the off-shell prescriptions can be traced back to the different energy transfers employed in each case. They can affect the results in different ways:

- For the off-shell prescriptions, the nucleon form factors F_1 and F_2 are functions of the real four-momentum transfer, i.e. $F_{1,2} = F_{1,2}(Q^2)$ with $Q^2 = \omega^2 - q^2$. However, for the ‘on-shell’ prescription the dependence of these form factors is taken to be $Q_{on-shell}^2 = \omega_{on-shell}^2 - q^2$. The dipole τ dependence of the electric and magnetic form factors considered in this work, explains why the discrepancy between $F_{1,2}(Q^2)$ and $F_{1,2}(Q_{on-shell}^2)$ increases for higher values of q and y . An alternative ‘on-shell’ prescription (not considered here) is to employ form factors $F_{1,2}(Q^2)$ in place of $F_{1,2}(Q_{on-shell}^2)$ with all else left unchanged.
- In the case of the Landau and Weyl gauges, because of the way of imposing current conservation (Weyl gauge) or not enforcing it (Landau), an additional dependence on the off-shell energy transfer ω enters in the single-nucleon responses. These are evaluated as $\mathcal{R}^L = (q/\omega)^2 \mathcal{S}^{33}$ and $\mathcal{R}^{TL} = 2\sqrt{2}(q/\omega) \mathcal{S}^{31}$ (coplanar kinematics) for the Weyl gauge, and as given by Eqs. (18,20) for the Landau gauge. For the ‘on-shell’ prescription, current conservation is fulfilled, and this additional dependence on ω does not enter. Obviously, in the case of the $CC2$ choice of the current such ω dependence is also contained within the current operator itself.

To finish the discussion of the unpolarized single-nucleon responses let us consider the results corresponding to the semi-relativistic reduction (long-dashed lines). We recall that any

comments made for the single-nucleon responses can be extended to the hadronic responses (when we neglect contributions from negative-energy projections), since the relativistic and non-relativistic momentum distributions are quite similar over the whole momentum range considered [13]. As shown, it agrees nicely with the relativistic calculations for the two interference responses, particularly for \mathcal{R}^{TT} . The discrepancy is at most of the order of $\sim 6\text{--}8\%$ for the high- p region, where the semi-relativistic reduction is less successful. The situation is clearly different for \mathcal{R}^L and \mathcal{R}^T where the divergence between relativistic and semi-relativistic results might be even of the order of $\sim 40\%$ for some specific kinematics for the higher p -values. Moreover, the semi-relativistic responses are almost constant over the entire range of p -values. This behaviour can easily be traced back by looking at the semi-relativistic expressions in Eqs. (26,27). The variation with p contained in the relativistic responses is due to the order- χ^2 terms entering in the relativistic expressions [23]. Finally, it is hard to deduce any clear systematics concerning the quality of the semi-relativistic reduction, and how it improves or gets worse with the momentum and energy transfers. What one can deduce is that, while a reasonable approximation for small missing momenta (say on the order of 100 MeV/c or smaller), such a semi-relativistic description does not seem to be adequate to describe the \mathcal{R}^L and \mathcal{R}^T responses at higher values of p . Even for intermediate p -values ($200 \leq p \leq 300$ MeV/c) the semi-relativistic reductions fail to some degree, as the deviations can be already of the order of $\sim 15\text{--}20\%$.

Polarized responses

The four recoil nucleon polarized responses that enter in the analysis of $(\vec{e}, e'\vec{p})$ reactions within PWIA and co-planar kinematics are shown in Figs. 9-12. The labels are the same as for the unpolarized responses. Some of the discussion already presented above for the unpolarized responses can be also applied to these polarized ones. Let us start by analyzing the uncertainty due to the choice of the current operator. As shown in the figures, in the case of the two purely transverse responses, $\mathcal{R}_t^{T'}$ and $\mathcal{R}_s^{T'}$, which do not depend on the gauge, the uncertainty is rather small for all of the $\{q, y\}$ -values selected. In the case of the interference TL responses (not shown), $\mathcal{R}_t^{TL'}$ and $\mathcal{R}_s^{TL'}$, we find that the Gordon ambiguity is also typically, but with some exceptions, relatively small for the Coulomb and Landau gauges. The same result holds for the Weyl gauge in $\mathcal{R}_t^{TL'}$, while the discrepancy introduced in $\mathcal{R}_s^{TL'}$ is significantly enhanced, in particular for large p -values.

The discussion of the gauge uncertainties follows similar trends to the ones presented for the unpolarized responses. Summarizing the basic results, one may conclude that the spread in the curves evaluated with the Coulomb and Landau gauges tends to be wider as y increases. On the contrary, the Weyl gauge results tend to come closer, as well as they do as q increases.

Regarding the ‘on-shell’ prescription (dotted line), the discussion follows the same trends already presented at length in the case of the unpolarized responses, and therefore we will not repeat them here. The reader is referred to the above discussion for details. We should only point out that the ‘on-shell’ approach gives very similar results to the off-shell ones in the case of small/medium q and negative y (see the results for $q = 500$ MeV/c and $y = -200$ MeV/c). An exception is the Weyl gauge whose results and general behaviour, as already

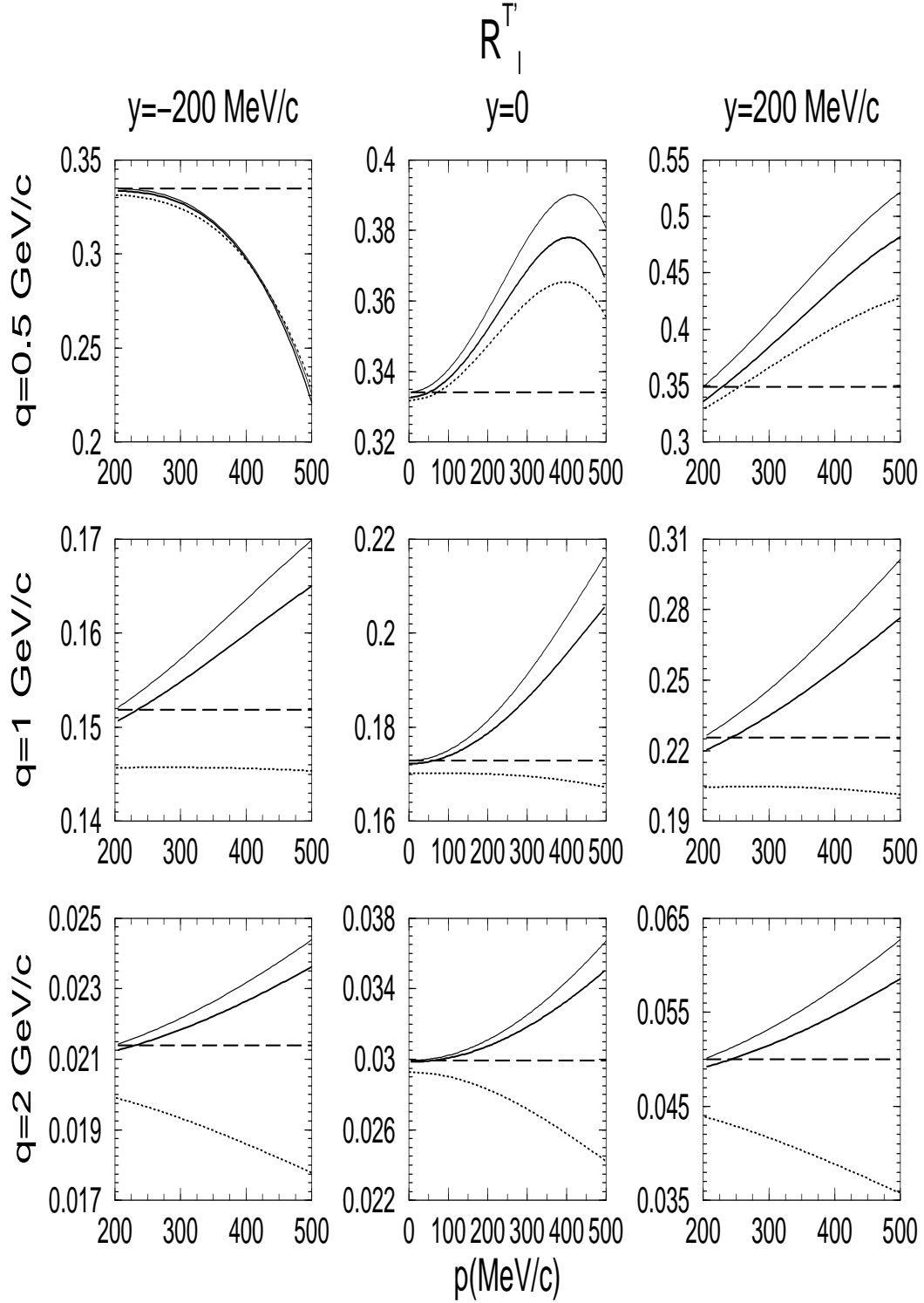


Figure 9: Same as Fig. 6, but for the polarized response $\mathcal{R}_l^{T'}$.

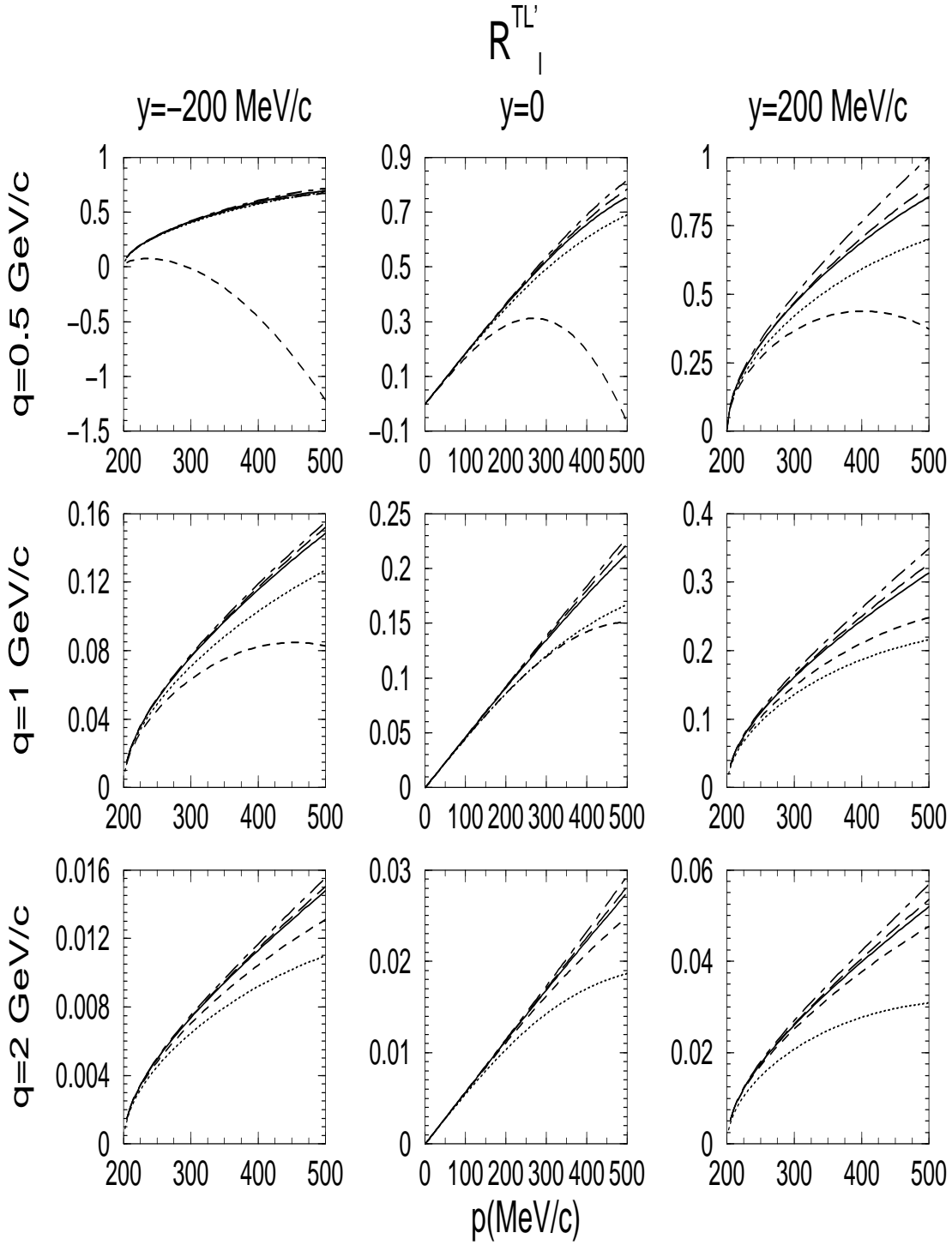


Figure 10: Same as Fig. 5, but for the response $\mathcal{R}_i^{TL'}$.

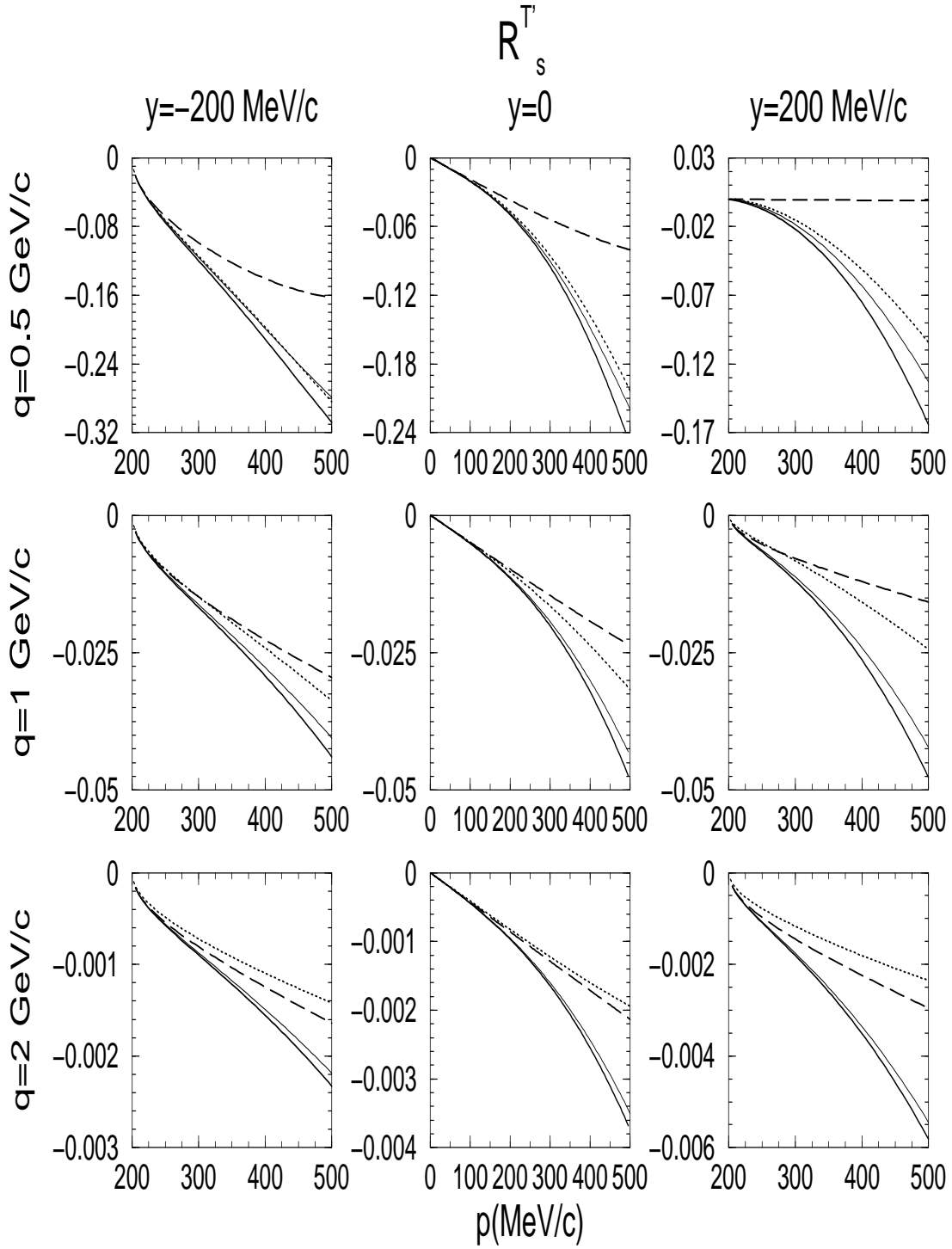


Figure 11: Same as Fig. 6, but for the response $\mathcal{R}_s^{T'}$.

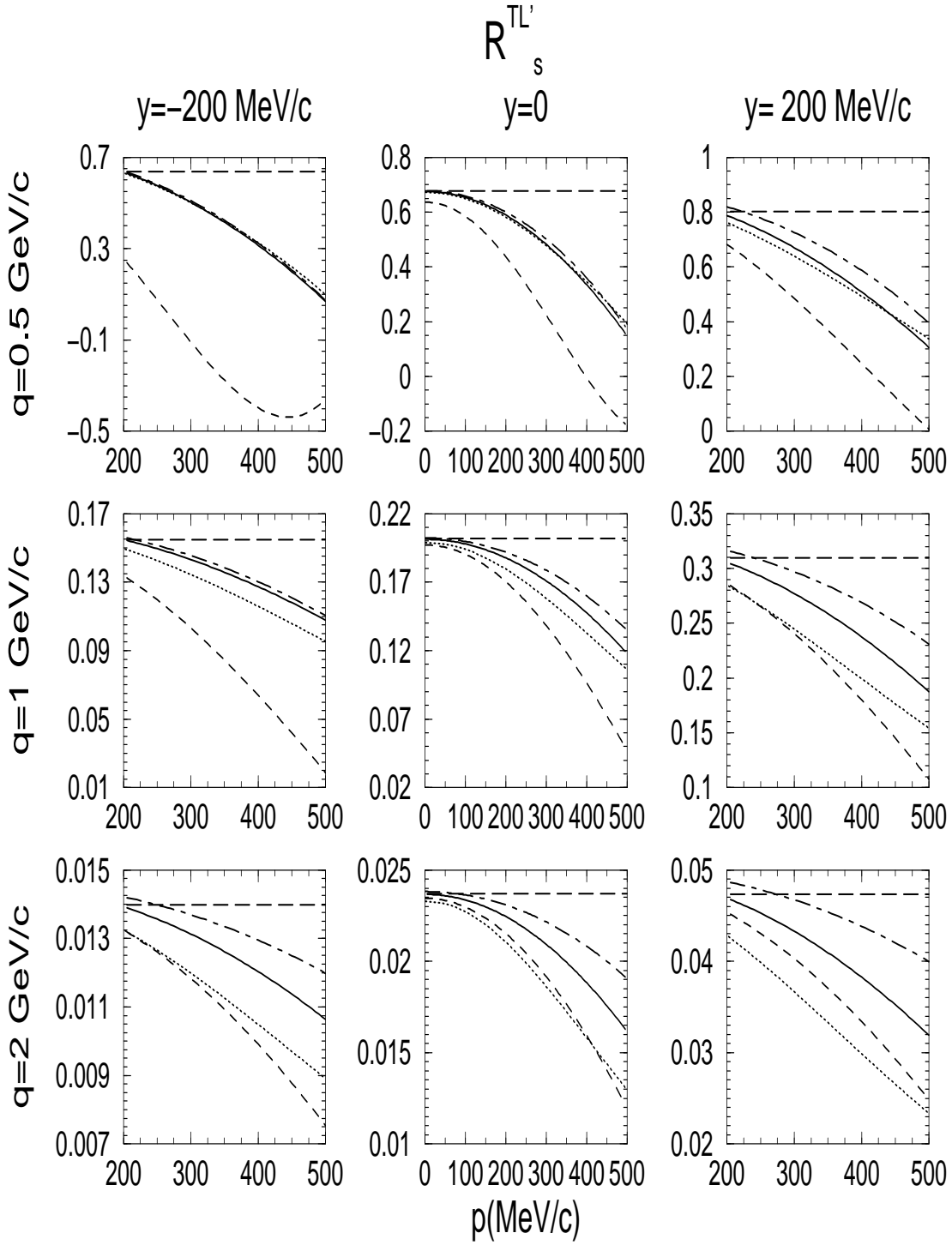


Figure 12: Same as Fig. 5, but for the response $\mathcal{R}_s^{TL'}$.

discussed, can be very different from Coulomb and Landau gauge results.

Finally, with regard to the behaviour of the semi-relativistic reductions for the polarized responses (long-dashed lines), the following conclusions can be drawn:

- The semi-relativistic reduction works nicely for $\mathcal{R}_i^{TL'}$. In fact, this polarized response is the one that shows the smallest kinematical relativistic effects. In particular, the relative difference between the semi-relativistic results and the $CC1^{(0)}$ prescription is less than $\sim 7\%$ even at high missing momenta. This behaviour echoes the one already observed for the unpolarized \mathcal{R}^{TL} and \mathcal{R}^{TT} responses. It is also interesting to point out the similarity between \mathcal{R}^{TL} and $\mathcal{R}_i^{TL'}$, particularly for large q , independent of the approach considered.
- The kinematical relativistic effects in the response $\mathcal{R}_i^{T'}$ are in general quite high for large missing momenta (for some particular kinematics they can be of the order of $\sim 20\text{--}30\%$). Only in the low- p region ($p < 200$ MeV/c) is a semi-relativistic reduction for this response acceptable, as the differences are less than $\sim 6\%$ (for $|y| = 200$ MeV/c this is true up to 250 MeV/c). This result is similar to the one seen for \mathcal{R}^L and \mathcal{R}^T . Note that the semi-relativistic expressions for \mathcal{R}^T and $\mathcal{R}_i^{T'}$ are identical (see Eqs. (27,30)). Moreover, the off- and ‘on-shell’ relativistic results for both responses, although different for low q ($q = 500$ MeV/c), tend to be very similar for large q (compare the two responses for $q = 2$ GeV/c).
- Finally, the largest kinematical relativistic effects are observed for the two sideways polarized responses, $\mathcal{R}_s^{T'}$ and $\mathcal{R}_s^{TL'}$, particularly for the latter, where they are typically of the order of $\sim 40\text{--}50\%$, and even much bigger for some specific off-shell prescriptions and large p values. This uncertainty is proven to diminish (for a given p) as q increases. As a conclusion, while for very small missing momenta the expansion procedure is not too bad, a semi-relativistic treatment is not suitable for these cases when intermediate-to-high values of p are considered; indeed, the differences from the relativistic results can be already as high as $\sim 25\%$ for $\mathcal{R}_s^{T'}$ and $\sim 15\%$ for $\mathcal{R}_s^{TL'}$ even for missing momenta as low as $p \sim 200$ MeV/c.

Summarizing, we may conclude that the sideways polarized responses are significantly affected by the kinematical relativistic effects. Moreover, once one has selected the recoil nucleon polarization direction (longitudinal versus sideways) class ‘1’ responses, $\mathcal{R}_i^{TL'}$ and $\mathcal{R}_s^{T'}$, seem to be less sensitive to relativistic kinematics than the corresponding class ‘0’ responses, $\mathcal{R}_s^{TL'}$ and $\mathcal{R}_i^{T'}$. This agrees with the general findings already presented for the unpolarized responses. It is important to point out, however, that kinematical relativistic effects seem to be more sensitive to the recoil nucleon polarization direction than to the response class type. Hence, an analysis based on semi-relativistic reductions should be taken very cautiously in some cases.

In context, we also note that a similar analysis has been performed in a parallel study of dynamical relativistic effects [12] and there a different pattern emerges. Without presenting any detail here (referring the reader to that other work) we summarize by stating that, as a general rule, we find that the less important the dynamical relativistic effects are found to be, the larger are the kinematical effects.

To finish the analysis in this section let us recall that the longitudinal polarized responses $\mathcal{R}_l^{T'}$ and $\mathcal{R}_l^{TL'}$ tend to be similar to the unpolarized ones, \mathcal{R}^T and \mathcal{R}^{TL} , respectively, for higher q -values. This result can be explained by noting that as q increases, the range of θ_N corresponding to $0 \leq p \leq 500$ MeV/c is significantly reduced. In other words, as q goes up the kinematics become closer to parallel kinematics, i.e., the θ_N -range covered within $0 \leq p \leq 500$ MeV/c is much smaller. This means that the higher the momentum q , the closer are the directions of \mathbf{q} and the longitudinal polarization \mathbf{l} aligned. In fact, in the limit case of parallel kinematics $\mathcal{R}_l^{TL'}$ and \mathcal{R}^{TL} are zero while \mathcal{R}^T and $\mathcal{R}_l^{T'}$ coincide.

4.2 Analysis of single-nucleon responses for parallel kinematics

In Figs. 13 and 14 we present the unpolarized and polarized responses that enter in $A(\vec{\epsilon}, e'\vec{p})B$ reactions within parallel kinematics and PWIA. Two choices of the dynamical variables have been selected: $\{p_N, \theta_N = 0, \mathcal{E} = 0, p\}$ and $\{q, \theta_N = 0, \mathcal{E} = 0, p\}$ (see Section 4 for details).

Within parallel kinematics and the PWIA only four responses survive in $(\vec{\epsilon}, e'\vec{N})$ processes, \mathcal{R}^L , \mathcal{R}^T , $\mathcal{R}_l^{T'}$ and $\mathcal{R}_s^{TL'}$. Moreover, \mathcal{R}^T and $\mathcal{R}_l^{T'}$ are proven to be identical in this case. Therefore, in the figures that follow we only present results for \mathcal{R}^L , \mathcal{R}^T and $\mathcal{R}_s^{TL'}$. Fig. 13 corresponds to the choice $\{p_N, \theta_N = 0\}$, while Fig. 14 corresponds to $\{q, \theta_N = 0\}$. In both cases we represent the responses for $\theta = 0$ and $\theta = 180^\circ$. In each graph we show the curves corresponding to the various off-shell prescriptions based on the $CC2$ current and the ‘on-shell’ approach. Again, although not shown in the graphs, we have also explored the behaviour for the $CC1$ prescriptions. The semi-relativistic reduction coincides with the $CC1^{(0)}$ prescription in parallel kinematics, as the expansion has been made in powers of $\chi \equiv (p/M_N) \sin \theta$, and this variable is strictly zero for this choice of kinematics. The labels are the same as in previous figures.

We start the discussion with the responses obtained by fixing the outgoing nucleon momentum p_N (Fig. 13). The results for strictly parallel kinematics are displayed in the two top panels. Here $q < p_N$ and higher p -values imply lower values of q . In this situation there exists a maximum value of p for which q comes close to ω , i.e. to the real photon point. In such a case, \mathcal{R}^L and $\mathcal{R}_s^{TL'}$ evaluated with the Landau gauge are divergent because of the term Q^2 entering in the denominator in the general expressions (18,23). When current conservation is imposed (Coulomb and Weyl gauges) the Q^2 factor cancels and the divergency disappears. Nevertheless, in this case using the popular off-shell prescriptions, as we do here, is highly suspect. The situation is clearly different within antiparallel kinematics (bottom panels). Here the larger the momentum p is the higher is the momentum transfer q .

The results in Fig. 13 show that off-shell uncertainties are clearly enhanced for strictly parallel kinematics. In particular, only the Weyl gauge present a different behaviour within antiparallel kinematics from the other prescriptions considered. This difference tends to diminish as p_N grows. On the contrary, the discrepancy between the various off-shell options explode for large p -values within the strictly parallel kinematics regime. Similar comments can be also applied to the ‘on-shell’ prescription: again the relative differences with the relativistic responses are much smaller within antiparallel kinematics. It is interesting to point out that the discrepancy between the ‘on-shell’ approach and the $CC1^{(0)}$ calculation grows (although less so for negative p) as p_N increases.

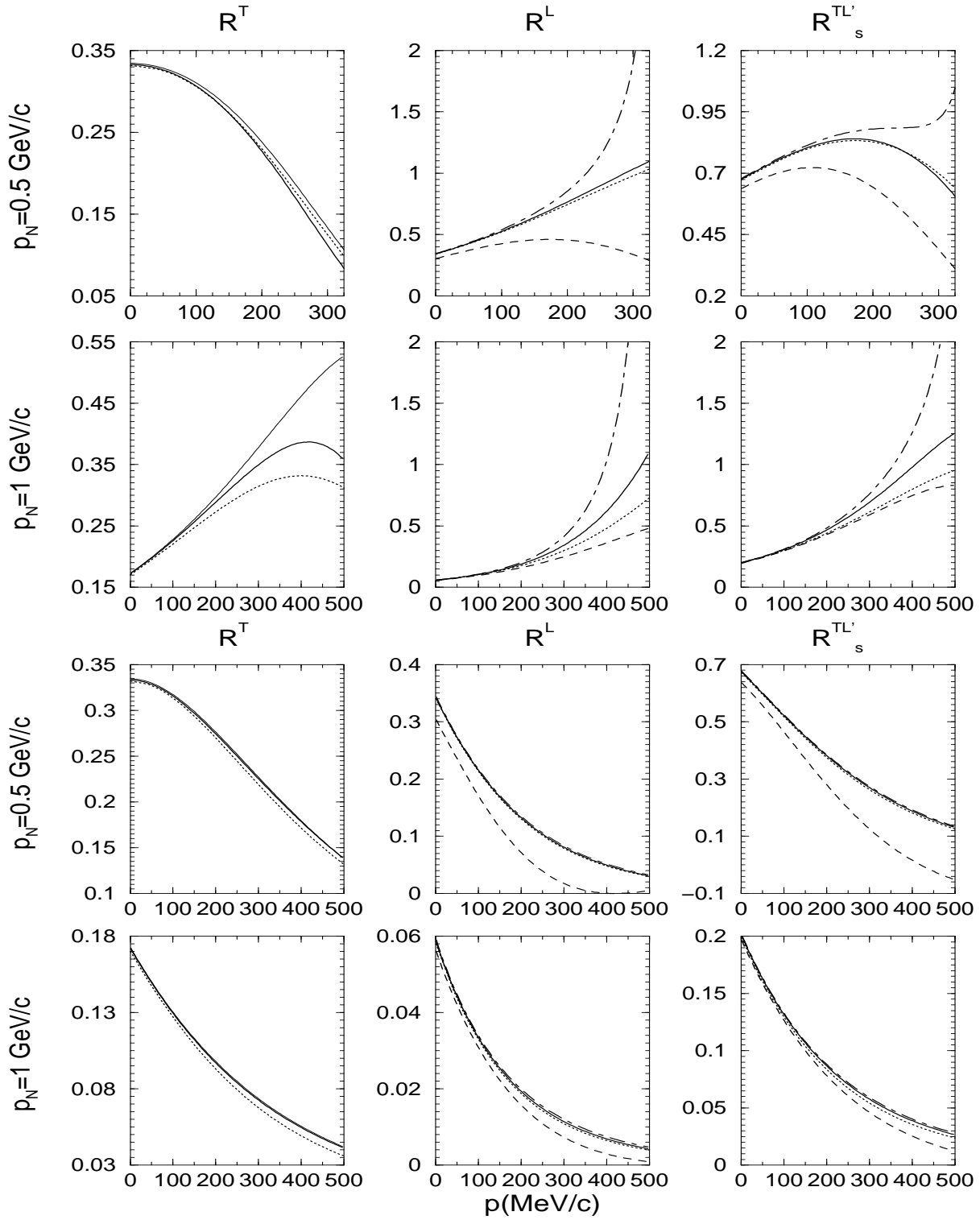


Figure 13: Single-nucleon responses in parallel kinematics. Results are shown for two values of the outgoing nucleon momentum. The two top panels correspond to strictly parallel kinematics, $\theta = 0$ (also called the positive p -region), while the two bottom panels correspond to antiparallel kinematics, $\theta = 180^\circ$ (negative p -region). The labels are the same as in Fig. 5, including the $CC1$ results (thin solid lines) for \mathcal{R}^T .

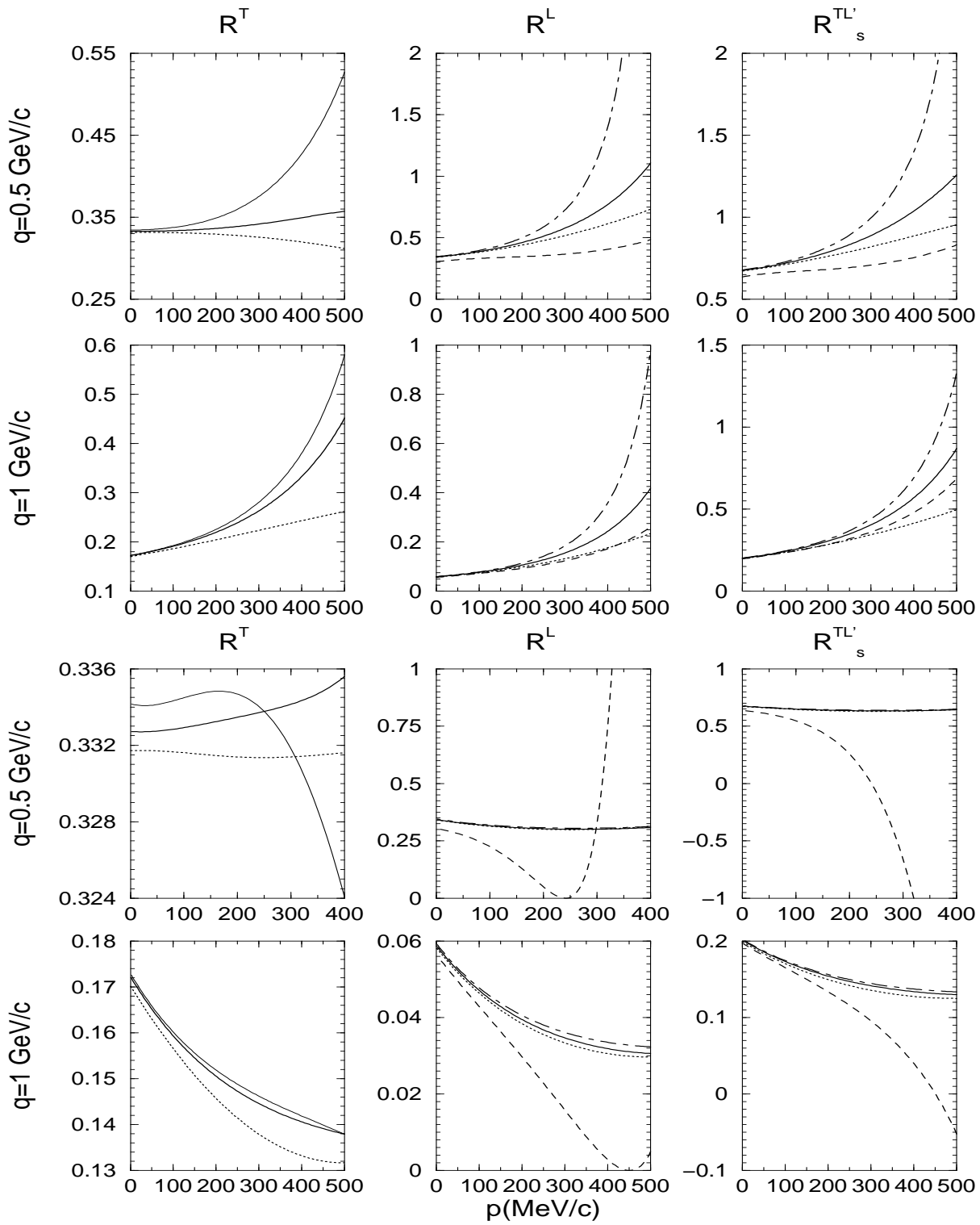


Figure 14: Same as Fig. 13, but for fixed q -values.

In Fig. 14 the responses for the $\{q, y\}$ choice are shown. The two top panels correspond to $\theta = 0$ and two bottom panels to $\theta = 180^\circ$. The general behaviour of the results for $\theta = 0$ follows similar trends to the one discussed in the previous case. In particular, the purely transverse response is very sensitive to the choice of the current as well as to the ‘on-shell’ approach for higher missing momenta. In the case of \mathcal{R}^L and $\mathcal{R}_s^{TL'}$ the main uncertainty is introduced by the gauge choice. The exploding behaviour shown by the Landau results for the highest p -values is again explained by the factor Q^2 entering in the denominator in Eqs. (18,23). In this situation (q -fixed) as p grows the outgoing nucleon momentum p_N also increases and consequently the energy transfer ω comes higher, approaching the value of the momentum transfer q , i.e., the real photon point. For antiparallel kinematics (bottom panels), increasing p implies decreasing p_N and hence ω being smaller. This also explains the totally different behaviour shown by the Weyl results in the longitudinal and transverse-longitudinal responses. Let us recall that the Weyl gauge implies that \mathcal{R}^L and $\mathcal{R}_s^{TL'}$ are evaluated by taking only the longitudinal (3) components of the single-nucleon tensors (current conservation is imposed) multiplied by a general factor (q/ω) or $(q/\omega)^2$. Thus as p grows the energy transfer ω goes down and the above factors may give a very important contribution (q -fixed). In particular, for $q = 500$ MeV/c the limit value $p = 500$ MeV/c corresponds to $p_N = 0$. The energy transfer is then simply given by $\omega = M_N + E_B - M_A$, which can be approximated by $E_S + \mathcal{E}$, a very small value compared with q .

Summarizing, we may conclude that within parallel kinematics the “safest” situation corresponds to $\theta = 180^\circ$ (antiparallel) fixing the kinetic energy of the outgoing nucleon. Unfortunately, since when compared with strictly parallel kinematics ($\theta = 0$) one has higher $|Q^2|$, smaller cross sections and more difficulty performing measurements under such conditions, fewer data exist for antiparallel kinematics. In the antiparallel case, apart from the Weyl gauge choice that maximizes the discrepancy, the results for the remaining off-shell and ‘on-shell’ prescriptions are all rather similar. The spread of the various approaches gets wider for antiparallel kinematics and q -fixed. Particularly, the Weyl gauge tends to explode for high p in the L and TL' responses. Finally, the behaviour of the responses for strictly parallel kinematics is rather similar in the two situations analyzed, p_N and q fixed. In both cases, the ambiguities introduced by the different approaches tend to be very high for large p -values. Moreover, as p reaches very high values one is moving close to the real photon point. In that case the Landau gauge responses diverge.

4.3 Transferred polarization asymmetries

In this section we analyze the transferred polarization asymmetries introduced in Eq. (10). These observables are given as ratios between polarized and unpolarized responses, where one hopes to gain different insight into the underlying physics from what may be revealed through the responses themselves. For instance, it may (or may not) be true that the polarization transfer asymmetries are less affected by FSI effects, by off-shell ambiguities, etc., than are the responses. One goal of this work is to explore briefly a few of these issues. In particular, there exists considerable interest in measurements of P'_l and P'_s as they may provide information on the structure of the nucleon in the nuclear medium. A more complete analysis of the off-shell and dynamical relativistic effects in these observables is presented

in [12], and hence here we focus mainly on the kinematical relativistic effects within PWIA.

In Figs. 15 and 16 we show results for P'_l and P'_s , respectively. Let us recall that the responses in PWIA factorize. This means that the transferred polarizations do not depend on the nuclear dynamics, and only the single-nucleon responses contribute. As is well-known, this constitutes a basic difference with respect to the relativistic plane-wave impulse approximation (RPWIA) [12, 13]. To simplify the discussion that follows we only present results for $\{q, y\}$ -fixed kinematics. The excitation energy \mathcal{E} and the azimuthal angle ϕ are taken to be zero. The electron scattering angle selected is $\theta_e = 30^\circ$, i.e., forward electron scattering. This kinematical situation maximizes the off-shell effects [12]. The labels of the curves in each graph are the same as those used for the single-nucleon responses.

We may summarize the basic findings as follows:

- The largest off-shell effects are introduced by the Weyl gauge (short-dashed lines). This is consistent with the results already observed for the single-nucleon responses. Moreover, the discrepancy between the Weyl results and the Landau or Coulomb responses tends to diminish for higher q . In contrast, the discrepancies between the remaining off-shell prescriptions are rather small for low q and negative y .
- Concerning the ‘on-shell’ approach (dotted line), the results obtained are rather similar to those for either the Coulomb or Landau gauges. Actually, they lie amongst the CCi^0 and $NCCi$ ($i = 1, 2$) results except for P'_l and $q = 2$ MeV/c; even in that case the off-shell uncertainty introduced by adding the ‘on-shell’ result remains quite small, as one can easily appreciate from the figures.
- The results obtained for the semi-relativistic reduction (long-dashed line) show that the kinematical relativistic effects may have a very important role to play, modifying completely the structure of the polarization asymmetries P'_l and P'_s for some kinematics. To be more specific, the semi-relativistic reductions compare less well with the relativistic results for the sideways polarization, as was expected from the fact that the sideways polarized responses were the most sensitive to kinematical relativistic effects. The only situations for which a semi-relativistic reduction may work reasonably well are the followings:
 - The low- p region ($p \leq 150$ MeV) when we are under quasielastic conditions where $y = 0$: the differences between relativistic and semi-relativistic results remain small (less than 10%) for all kinematics except for the case $q = 500$ MeV/c for P'_l . Going to higher missing momenta implies finding larger kinematical effects (bigger than 10%) except for the $q = 1, 2$ MeV/c cases in P'_l , for which the semi-relativistic reduction approximates the relativistic results rather well (within 6% up to $p = 350$ MeV/c).
 - For the $y = -200$ MeV/c cases, the kinematical relativistic effects are small up to $p = 250$ MeV/c in the case of P'_s and up to $p = 350$ MeV/c for P'_l (again except for $q = 500$ MeV/c). However, for $y = 200$ MeV/c, the semi-relativistic reductions differ significantly from the relativistic results for both observables.

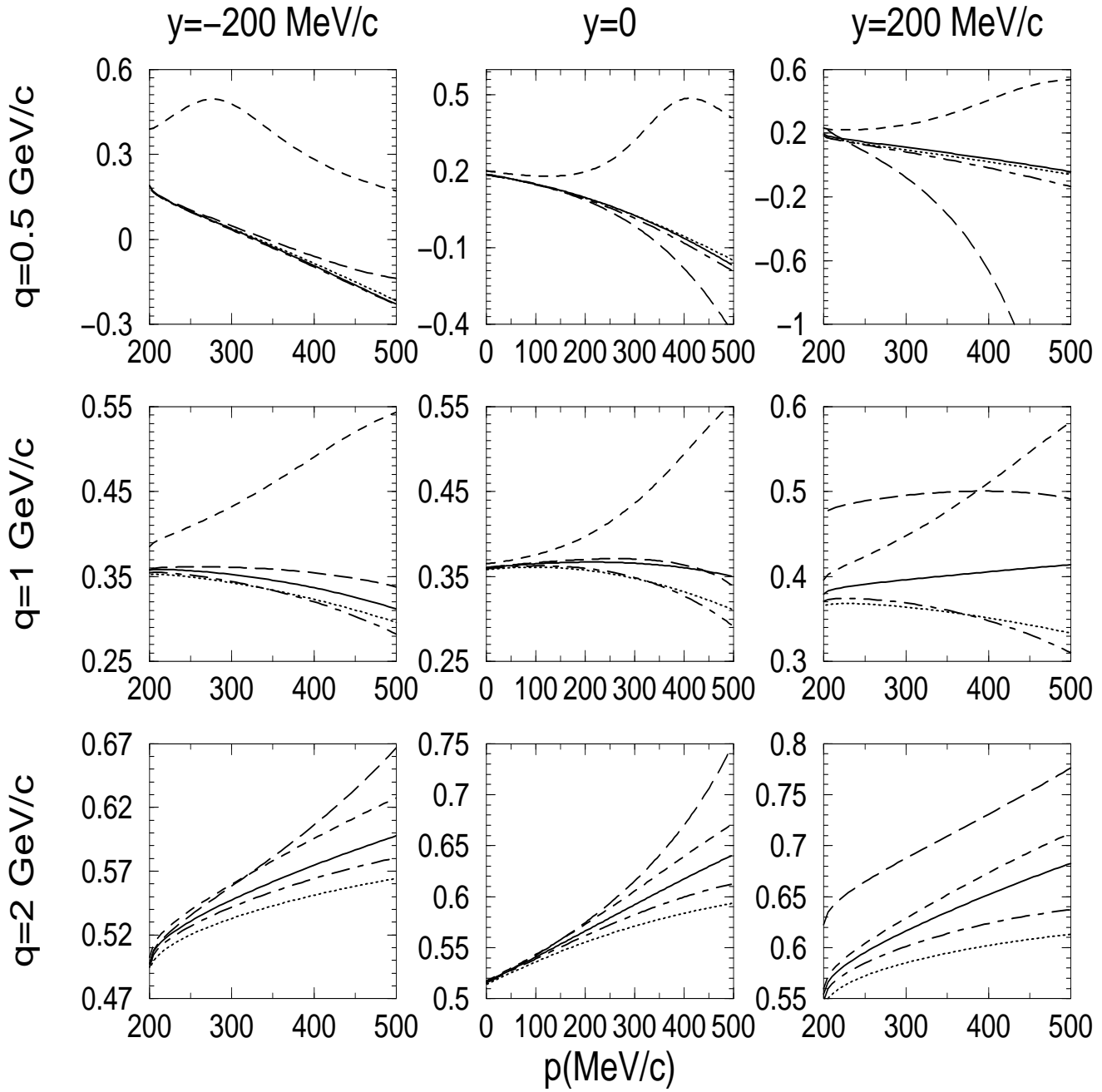


Figure 15: Transferred polarization asymmetry for longitudinal spin direction. The labels are as in Fig. 5.

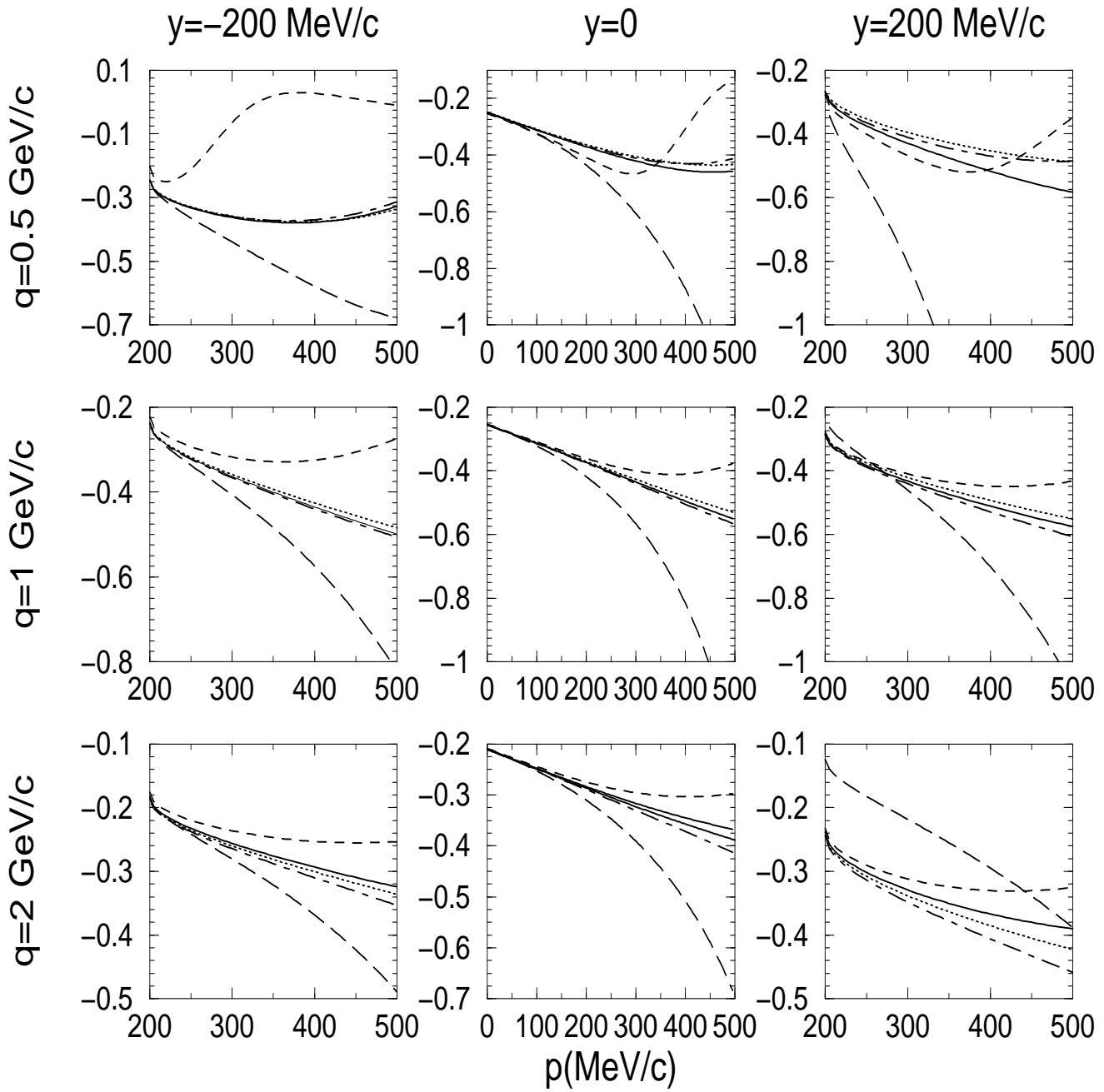


Figure 16: Same as Fig. 15, but for the transferred polarization asymmetry for the sideways spin direction.

Consequently, one has to be very careful before using a semi-relativistic reduction for these observables, given that only in particular regimes does it provide results that are similar to the relativistic ones. Even for relatively small p -values one can find rather important kinematical relativistic effects. Finally, it is interesting to point out that the semi-relativistic approach may even yield non-physical results, transfer polarizations smaller than -1.

Summarizing, we may conclude in general that the transferred polarization asymmetries evaluated with the Landau and Coulomb prescriptions do not show large differences; they are at most of the order of $\sim 1.5\%$ for $p \approx 100$ MeV/c, where the cross section and response functions are mainly located in the case of ^{16}O . The Weyl gauge on the contrary gives rise to results that sometimes differ completely. This is in accordance with the results discussed for the responses in the previous section and it also agrees with several previous papers [12, 13, 23]. The ‘on-shell’ approach in general fits rather nicely with the off-shell results based on either Landau or Coulomb gauges.

Taking into account the previous comments on semi-relativistic reductions, it turns out that even in approximation schemes where the momentum and energy transfers are treated exactly it does not seem to be very appropriate to employ such analyses of the transferred polarization observables for the $\{q, y\}$ -fixed kinematics, except perhaps at rather low missing momenta.

5 Summary and conclusions

In this work our interest has been focused on the analysis of kinematical relativistic effects and off-shell uncertainties in $A(\vec{e}, e'\vec{N})B$ reactions within the context of the plane-wave impulse approximation (PWIA). In other work being done in parallel we have also been exploring dynamical relativistic effects using the relativistic plane-wave impulse approximation (RPWIA) [12]. The basic difference between RPWIA and PWIA is that the latter does not include the role played by the enhancement of the negative-energy components of the bound nucleon wave function. A crucial consequence of this is that within PWIA the response functions (differential cross section) factorize into single-nucleon responses (single-nucleon cross section) and the spectral function or momentum distribution, the latter containing the entire dependence on the nuclear dynamics. Therefore, observables given as ratios of responses or cross sections, such as the transferred polarization asymmetries, do not depend on the nuclear dynamics in PWIA.

In this work we have presented a systematic analysis for a variety of kinematical conditions of all of the single-nucleon responses that enter in the description of $A(\vec{e}, e'\vec{N})B$ processes within PWIA. In particular, we have analyzed the results obtained not only for the quasielastic peak conditions, but also moving far above or below the peak. In each kinematical situation a very wide set of different options has been considered:

- First, concerning fully-relativistic PWIA calculations: here various alternatives to deal with the off-shell character of the bound nucleon have been explored. They are connected with the current operator choice and the current conservation property. Addi-

tionally, within this scheme, we have also analyzed the so-called ‘on-shell’ prescription in which the bound nucleon is forced to be on-shell.

- Second, we have also presented a detailed study of the reductions of the various responses treating exactly the problem of the energy and momentum transfers, but expanding in initial state momenta divided by the nucleon mass – indeed, these are not the traditional non-relativistic expansion schemes and we have highlighted this fact by calling them “semi-relativistic” expansions. Different semi-relativistic alternatives have been explored. This analysis gives us a clear image of the role played by the kinematical relativistic effects in the various observables that are accesible in $(\vec{e}, e'\vec{N})$ reactions. Moreover, the semi-relativistic reduction has allowed us to classify the responses into three basic categories according to the leading order term in the expansion: class “0” (leading-order χ^0), class “1” (χ^1) and class “2” (χ^2) responses. We have found this to be a very natural way to classify the responses and, even more importantly, it allows us to simplify the discussion of the role of the kinematical and dynamical relativistic effects.

Concerning the results for $\{q, y\}$ -fixed kinematics, we may summarize the basic conclusions as follows. The largest off-shell uncertainties are introduced in general by the prescriptions based on the Weyl gauge. This agrees with the general discussion already presented in [12, 13]. Furthermore, we also find that the discrepancy between the Weyl results and the Landau and Coulomb gauge results becomes smaller for higher values of the momentum transfer q and increasing values of the scaling variable y . With regard to the results evaluated with the Landau and Coulomb gauges, the discrepancy between them is much smaller, increasing slightly as y goes from negative to positive values. Finally, the ambiguity introduced by the choice of the current operator is also well under control. The ‘on-shell’ approach gives rise to results which are rather similar to the off-shell ones based on the Coulomb and Landau gauges for q and y small. We have revealed the reason for this discrepancy and have explained why it increases for higher q and y -values.

Kinematical relativistic effects are clearly made evident when comparing the semi-relativistic calculation with the various off-shell results. Here we find as a general rule that the discrepancy between the two approaches is significantly smaller for higher class type responses, i.e., kinematical relativistic effects are very small for class “2” responses, increase slightly for class “1” responses, and are the largest for class “0” responses. This behaviour is strictly true in the case of the four unpolarized responses: \mathcal{R}^L , \mathcal{R}^T (class “0”), \mathcal{R}^{TL} (class “1”) and \mathcal{R}^{TT} (class “2”). For the recoil nucleon polarized responses, the direction of the spin polarization plays also a crucial role in the determination of the relativistic effects, and one should take into account both ingredients, polarization direction and response class type. We have found that kinematical relativity shows a stronger sensitivity to the recoil nucleon polarization direction than to the response class type. However, it is important to point out that for a fixed polarization direction, the above statement on the connection between kinematical relativistic effects and class type responses remains valid.

In this work we have also presented a careful analysis of the results corresponding to parallel kinematics. Here one should distinguish between strictly parallel kinematics, i.e., \mathbf{p} , \mathbf{q} and \mathbf{p}_N parallel, and antiparallel kinematics, i.e., \mathbf{p} opposite to \mathbf{q} and \mathbf{p}_N . Two different

choices for the dynamical variables that specify the response functions have been considered. In the former the outgoing nucleon momentum p_N is fixed, and in the latter the momentum transfer q is assumed fixed. The results show very clearly that the situation corresponding to antiparallel kinematics and p_N -fixed minimizes the off-shell uncertainties. On the contrary, the three remaining regimes, strictly parallel kinematics with p_N fixed and the two kinematics corresponding to q -fixed, present large uncertainties. In particular, within strictly parallel kinematics, as the missing momentum p increases one is approaching the real photon point for which the difference between the various prescriptions can explode — in fact, the Landau results diverge in that case.

The transferred polarization asymmetries, P'_l and P'_s , may provide information on nucleon structure in the nuclear medium, and accordingly these have been also analyzed in the case of $\{q, y\}$ -fixed kinematics and forward electron scattering. As is well-known, this situation maximizes the off-shell uncertainties. We find that the results for the off-shell prescriptions based on the Landau and Coulomb gauges and the ‘on-shell’ approach present a similar behaviour whose relative differences depend on the specifics of the kinematics. The Weyl prescription produces results that are completely different, particularly for low- q and negative- y . This discrepancy tends to diminish for higher q . Finally, the kinematical relativistic effects are also shown to be very important, in particular for the sideways nucleon polarization direction. In this case, the semi-relativistic results present a behaviour that differs significantly from all other calculations independently of the specific kinematics selected. The semi-relativistic approach may even lead to unphysical results $|P'_s| > 1$. Although the sensitivity of P'_l to kinematical relativistic effects is reduced, one still observes very important deviations even at the quasielastic peak.

Although FSI and other ingredients such as two-body meson exchange-currents may have additional important effects in the analysis of $(\vec{e}, e'\vec{N})$ observables (work along this line is presently in progress), some of the results presented here within PWIA are by themselves very illustrative of the uncertainties introduced by different approximations. In particular, the results for the transferred polarization asymmetries tell us that semi-relativistic treatments may not be adequate when describing such observables even for low- q and quasielastic peak conditions. Hence great caution should be taken when distorted-wave impulse approximation (DWIA) calculations based on semi-relativistic — or, even more so, non-relativistic — reductions of the current are used to describe experimental transferred polarization asymmetries.

Acknowledgements

This work was partially supported by funds provided by DGICYT (Spain) under Contracts Nos. PB/98-1111, PB/98-0676 and the Junta de Andalucía (Spain) and in part by the U.S. Department of Energy under Cooperative Research Agreement No. DE-FC02-94ER40818. M.C.M acknowledges support from a fellowship from the Fundación Cámara (University of Sevilla). J.A.C. also acknowledges financial support from MEC (Spain) for a sabbatical stay at MIT (PR2001-0185). The authors thank E. Moya, J.M. Udías and J.R. Vignote for their helpful comments.

Appendix A

In this appendix we present the explicit expressions for the symmetric and antisymmetric terms of the single-nucleon tensor $\mathcal{W}^{\mu\nu}$ that enters in the analysis of $A(\vec{e}, e'\vec{N})B$ reactions withing PWIA for both current operators, $CC1$ and $CC2$, as well as the analytic expressions for the polarized single-nucleon $CC1^{(0)}$ and $CC2^{(0)}$ responses. The tensors are given as

- **CC1 current**

$$\begin{aligned} \mathcal{S}^{\mu\nu} &= \frac{1}{2M_N^2} \left\{ (F_1 + F_2)^2 \left(\bar{P}^\mu P_N^\nu + \bar{P}^\nu P_N^\mu + \frac{\bar{Q}^2}{2} g^{\mu\nu} \right) \right. \\ &\quad \left. - \left[(F_1 + F_2)F_2 - \frac{F_2^2}{2} \left(1 - \frac{\bar{Q}^2}{4M_N^2} \right) \right] C^\mu C^\nu \right\} \end{aligned} \quad (38)$$

$$\begin{aligned} \mathcal{A}^{\mu\nu} &= \frac{i}{2M_N^2} \left\{ M_N^2 (F_1 + F_2)^2 \varepsilon^{\alpha\beta\mu\nu} S_{N\alpha} \bar{Q}_\beta \right. \\ &\quad \left. + (F_1 + F_2) \frac{F_2}{2M_N} \left(C^\mu \varepsilon^{\alpha\beta\gamma\nu} - C^\nu \varepsilon^{\alpha\beta\gamma\mu} \right) \bar{P}_\alpha P_{N\beta} S_{N\gamma} \right\} \end{aligned} \quad (39)$$

- **CC2 current**

$$\begin{aligned} \mathcal{S}^{\mu\nu} &= \frac{1}{2M_N^2} \left\{ F_1^2 \left(\bar{P}^\mu P_N^\nu + \bar{P}^\nu P_N^\mu + \frac{\bar{Q}^2}{2} g^{\mu\nu} \right) + F_1 F_2 \left(Q \cdot \bar{Q} g^{\mu\nu} - \frac{\bar{Q}^\mu Q^\nu + \bar{Q}^\nu Q^\mu}{2} \right) \right. \\ &\quad + \frac{F_2^2}{4M_N^2} \left[P_N \cdot Q \left(\bar{P}^\mu Q^\nu + \bar{P}^\nu Q^\mu \right) + \bar{P} \cdot Q \left(P_N^\mu Q^\nu + P_N^\nu Q^\mu \right) - Q^2 \left(P_N^\mu \bar{P}^\nu + P_N^\nu \bar{P}^\mu \right) \right. \\ &\quad \left. \left. - \left(2M_N^2 - \frac{\bar{Q}^2}{2} \right) Q^\mu Q^\nu + g^{\mu\nu} \left(2M_N^2 Q^2 - \frac{Q^2 \bar{Q}^2}{2} - 2P_N \cdot Q \bar{P} \cdot Q \right) \right] \right\} \end{aligned} \quad (40)$$

$$\begin{aligned} \mathcal{A}^{\mu\nu} &= \frac{i}{2M_N^2} \left\{ -M_N F_1^2 \varepsilon^{\alpha\beta\mu\nu} \bar{Q}_\alpha S_{N\beta} \right. \\ &\quad + \frac{F_1 F_2}{M_N} \left[\varepsilon^{\alpha\beta\mu\nu} \left(\bar{P} \cdot Q P_{N\alpha} S_{N\beta} - M_N^2 Q_\alpha S_{N\beta} \right) + \frac{1}{2} \left(Q^\mu \varepsilon^{\alpha\beta\gamma\nu} - Q^\nu \varepsilon^{\alpha\beta\gamma\mu} \right) S_{N\alpha} P_{N\beta} \bar{P}_\gamma \right] \\ &\quad \left. - \frac{F_2^2}{4M_N} \left[\varepsilon^{\alpha\beta\mu\nu} \left(2\bar{P} \cdot Q S_{N\alpha} Q_\beta + Q^2 C_\alpha S_{N\beta} \right) + \left(Q^\mu \varepsilon^{\alpha\beta\gamma\nu} - Q^\nu \varepsilon^{\alpha\beta\gamma\mu} \right) S_{N\alpha} C_\beta Q_\gamma \right] \right\}, \end{aligned} \quad (41)$$

where we have defined $C^\mu \equiv (\bar{P} + P_N)^\mu$.

Axis	$\mu = 0$	$\mu = 1$	$\mu = 2$	$\mu = 3$
l	$\sqrt{\gamma_N^2 - 1}$	$\frac{\gamma_N \chi}{\sqrt{\gamma_N^2 - 1}}$	0	$\frac{\gamma_N(\chi' + 2\kappa)}{\sqrt{\gamma_N^2 - 1}}$
s	0	$\frac{\chi' + 2\kappa}{\sqrt{\gamma_N^2 - 1}}$	0	$-\frac{\chi}{\sqrt{\gamma_N^2 - 1}}$
n	0	0	1	0

Table 1: Components of the spin four-vector $S_N^\mu(\mathbf{l}, \mathbf{s}, \mathbf{n})$ in the laboratory system (see text for the notation).

By using the expressions given in Eqs. (22,23) and referring the recoil nucleon spin four-vector S_N^μ to the coordinate system defined by the axes **l**, **s** and **n** (see Table 1), it is possible to write down in a very compact form specific answers for the polarized single-nucleon $CC1^{(0)}$ and $CC2^{(0)}$ responses. They are given as

$$\begin{aligned} \mathcal{R}_l^{T'} &= \frac{2}{\sqrt{\gamma_N^2 - 1}} \left\{ (F_1 + F_2) \left[\frac{\xi \bar{\tau}}{\kappa} \left(\gamma_N F_1 + \bar{\lambda} F_2 \sqrt{\frac{\rho_1 + \rho_2}{2}} \right) - \kappa \left(F_1 - \bar{\tau} \sqrt{\frac{\rho_1 + \rho_2}{2}} F_2 \right) \right] \right. \\ &- \left. \frac{\bar{\tau}}{\kappa} \sqrt{\frac{\rho_2 - \rho_1}{2}} F_2 \left[\kappa \gamma_N \left(F_1 - \bar{\tau} \sqrt{\frac{\rho_1 + \rho_2}{2}} F_2 \right) - \frac{\xi}{\kappa} \bar{\tau} \left(F_1 - (\xi \gamma_N - 1) F_2 \sqrt{\frac{\rho_1 + \rho_2}{2}} \right) \right] \right\} \end{aligned} \quad (42)$$

$$\begin{aligned} \mathcal{R}_s^{T'} &= \frac{2\chi}{\sqrt{\gamma_N^2 - 1}} \left\{ (F_1 + F_2) \left[\bar{\lambda} F_1 - \gamma_N \bar{\tau} F_2 \sqrt{\frac{\rho_1 + \rho_2}{2}} \right] \right. \\ &- \left. \frac{\bar{\tau}}{\kappa} \sqrt{\frac{\rho_2 - \rho_1}{2}} F_2 \left[F_1 (\xi \gamma_N - 1) + \bar{\tau} F_2 \sqrt{\frac{\rho_1 + \rho_2}{2}} \right] \right\} \end{aligned} \quad (43)$$

$$\begin{aligned} \mathcal{R}_l^{TL'} &= \frac{2\sqrt{2}\kappa\chi}{\sqrt{\gamma_N^2 - 1}} \left\{ (F_1 + F_2) \left[(\gamma_N F_1 + \bar{\lambda} F_2) + \gamma_N \bar{\tau} F_2 \left(1 - \sqrt{\frac{\rho_1 + \rho_2}{2}} \right) \right] \right. \\ &+ \left. \frac{\bar{\tau}}{\kappa} \sqrt{\frac{\rho_2 - \rho_1}{2}} F_2 \left[(1 - \bar{\lambda} \gamma_N) F_1 - (\gamma_N^2 - 1) F_2 \right] \right\} \cos \phi \end{aligned} \quad (44)$$

$$\begin{aligned} \mathcal{R}_s^{TL'} &= \frac{2\sqrt{2}}{\sqrt{\gamma_N^2 - 1}} \left\{ (F_1 + F_2) \left[\xi \left(\bar{\lambda} F_1 - \gamma_N \bar{\tau} F_2 \sqrt{\frac{\rho_1 + \rho_2}{2}} \right) + \kappa^2 (F_1 + F_2) \right] \right. \\ &- \left. \frac{\bar{\tau}}{\kappa} F_2 \sqrt{\frac{\rho_2 - \rho_1}{2}} \left[(\xi (\gamma_N^2 - 1) - \gamma_N \kappa^2) F_1 + \bar{\lambda} (\xi^2 - \kappa^2) F_2 \right] \right\} \cos \phi \end{aligned}$$

(45)

$$\mathcal{R}_n^{TL'} = -2\sqrt{2} \left\{ \kappa(F_1 + F_2) \left[F_1 - \bar{\tau} F_2 \sqrt{\frac{\rho_1 + \rho_2}{2}} \right] - \frac{\xi^2}{\kappa^2} \bar{\tau} \bar{\lambda} \sqrt{\frac{\rho_2 - \rho_1}{2}} F_1 F_2 \right\} \sin \phi, \quad (46)$$

where we have introduced the usual dimensionless variables: $\chi \equiv \frac{p}{M_N} \sin \theta$, $\kappa \equiv \frac{q}{2M_N}$, $\bar{\lambda} \equiv \frac{\bar{\omega}}{2M_N}$, $\gamma_N \equiv \frac{E_N}{M_N}$, $\xi \equiv \frac{E_N + \bar{E}}{2M_N}$ and $\bar{\tau} \equiv \frac{|Q^2|}{4M_N^2}$. More details on these variables and the relations held between them are given in [23]. For compactness the above expressions have been written introducing the parameters ρ_1 and ρ_2 (see [23] for details). For the $CC1^{(0)}$ prescription one has $\rho_1 = \rho_2 = 1$, whereas for $CC2^{(0)}$ one has $\rho_1 = \tau/\bar{\tau}$ and $\rho_2 = 2[1 + \bar{\lambda}(\bar{\lambda} - \lambda)/\tau]^2 - \rho_1$ with $\lambda \equiv \frac{\omega}{2M_N}$ and $\tau \equiv \frac{|Q^2|}{4M_N^2}$. Note that for the $CC1^{(0)}$ prescription one has $\rho_2 - \rho_1 = 0$, and consequently the single-nucleon responses simplify considerably.

References

- [1] S. Boffi, C. Giusti, F.D. Pacati, M. Radici, “Electromagnetic Response of Atomic Nuclei”, (Oxford-Clarendon Press, 1996); Phys. Rep. **226** (1993).
- [2] J.J. Kelly, Adv. Nucl. Phys. V 23 (1996) 77.
- [3] S. Frullani and J. Mougey, Adv. Nucl. Phys. 14 (1985).
- [4] A. Picklesimer and J.W. Van Orden, Phys. Rev. **C35** (1987) 266.
- [5] A. Picklesimer and J.W. Van Orden, Phys. Rev. **C40** (1989) 290.
- [6] J.M Udías, P. Sarriguren, E. Moya de Guerra, E. Garrido, J.A. Caballero, Phys. Rev. **C48** (1993) 2731.
- [7] J.M Udías, P. Sarriguren, E. Moya de Guerra, E. Garrido, J.A. Caballero, Phys. Rev. **C51** (1995) 3246.
- [8] J.M. Udías, P. Sarriguren, E. Moya de Guerra, J.A. Caballero, Phys. Rev. **C53** (1996) R1488.
- [9] J.M. Udías, J.A. Caballero, E. Moya de Guerra, J.E. Amaro, T.W. Donnelly, Phys. Rev. Lett. **83** (1999) 5451.
- [10] J.M. Udías, J.A. Caballero, E. Moya de Guerra, J.R. Vignote, A. Escuderos, Phys. Rev. **C64** (2001) 024614.
- [11] Y. Jin, D.S. Onley, Phys. Rev. **C50** (1994) 377.
- [12] M.C. Martínez, J.A. Caballero, T.W. Donnelly, submitted to Nucl. Phys. **A** (2001).

- [13] J.A. Caballero, T.W. Donnelly, E. Moya de Guerra, J.M. Udías, Nucl. Phys. **A632** (1998) 323.
- [14] J.A. Caballero, T.W. Donnelly, E. Moya de Guerra, J.M. Udías, Nucl. Phys. **A643** (1998) 189.
- [15] S. Gardner, J. Piekarewicz, Phys. Rev. **C50** (1994) 2822.
- [16] M.C. Martínez et al., in preparation (2002).
- [17] J.E. Amaro, J.A. Caballero, T.W. Donnelly, A.M. Lallena, E. Moya de Guerra, J.M. Udías, Nucl. Phys. **A602** (1996) 263; **A611** (1996) 163.
- [18] J.E. Amaro, M.B. Barbaro, J.A. Caballero, T.W. Donnelly, A. Molinari, Nucl. Phys. **A643** (1998) 349.
- [19] A.S. Raskin, T.W. Donnelly, Ann. Phys. **191** (1989) 78.
- [20] D.B. Day, J.S. McCarthy, T.W. Donnelly, I. Sick, Ann. Rev. Nucl. and Part. Sci. **40** (1990) 357; T.W. Donnelly, “The Atomic Nucleus Observed with Electromagnetic Probes”, Oromana Int. Summerschool on Nucl. Phys., Seville (2000), published by J.M. Arias and M. Lozano in “An Advanced Course in Modern Nuclear Physics”, (Springer, 2001), 39-69.
- [21] T.W. Donnelly, I. Sick, Phys. Rev. **C60** (1999) 065502.
- [22] C. Giusti, F.D. Pacati, Nucl. Phys. **A504** (1989) 685.
- [23] J.A. Caballero, T.W. Donnelly, G.I. Poulis, Nucl. Phys. **A555** (1993) 709.
- [24] H.W.L. Naus, S. Pollock, J.H. Koch, U. Oelfke, Nucl. Phys. **A509** (1990) 717; S.J. Pollock, H.W.L. Naus, J.H. Koch, Phys. Rev. **C53** (1996) 2304.
- [25] T. de Forest, Nucl. Phys. **A392** (1983) 232.
- [26] S. Jeschonnek, T.W. Donnelly, Phys. Rev. **C57** (1998) 2438.